Journal of Medicinal Chemistry

Article

Cite This: J. Med. Chem. 2019, 62, 1231−1245

pubs.acs.org/jmc

Design of Novel Inhibitors of Human Thymidine Phosphorylase: Synthesis, Enzyme Inhibition, in Vitro Toxicity, and Impact on Human Glioblastoma Cancer

Nathalia D. de Moura Sperotto,[†,‡,○] Candida Deves Roth,[†,○] Valnês S. Rodrigues-Junior,[†] Christiano Ev Neves,[†] Fávero Reisdorfer Paula,[#] Adilio da Silva Dadda,[†] Pedro Bergo,[†] Talita Freitas de Freitas,[†] Fernanda Souza Macchi,[†,§] Sidnei Moura,[▽] Ana Paula Duarte de Souza,[∥] Maria Martha Campos,[‡,§,⊥] Cristiano Valim Bizarro,[†,§] Diógenes Santiago Santos,[†,§] Luiz Augusto Basso,*[,†,‡,§] and Pablo Machado*[,†,§]

[†]Centro de Pesquisas em Biologia Molecular e Funcional, Instituto Nacional de Ciência e Tecnologia em Tuberculose, [‡]Programa de Pós-Graduação em Medicina e Ciências da Saúde, [§]Programa de Pós-Graduação em Biologia Celular e Molecular, [∥]Laboratório de Imunologia Clínica e Experimental, Centro Infant, and [⊥]Centro de Pesquisa de Toxicologia e Farmacologia, Pontifícia Universidade Católica do Rio Grande do Sul, 90616-900 Porto Alegre, RS, Brazil

[#]Laboratório de Desenvolvimento e Controle de Qualidade em Medicamentos, Universidade Federal do Pampa, 97508-000 Uruguaiana, RS, Brazil

[▽]Laboratório de Produtos Naturais e Sintéticos, Instituto de Biotecnologia, Universidade de Caxias do Sul, 95070-560 Caxias do Sul, RS, Brazil

Supporting Information

ABSTRACT: Overexpressed human thymidine phosphorylase (hTP) has been associated with cancer aggressiveness and poor prognosis by triggering proangiogenic and antiapoptotic signaling. Designed as transition-state analogues by mimicking the oxacarbenium ion, novel pyrimidine-2,4-diones were synthesized and evaluated as inhibitors of hTP activity. The most potent compound (**8g**) inhibited hTP in the submicromolar range with a noncompetitive inhibition mode with both thymidine and inorganic phosphate substrates. Furthermore, compound **8g** was devoid of apparent toxicity to a panel of mammalian cells, showed no genotoxicity signals, and had low probability of drug−drug interactions and moderate in vitro metabolic rates. Finally, treatment with **8g** (50 mg/(kg day)) for 2 weeks (5 days/week) significantly reduced tumor growth using an in vivo glioblastoma model. To the best of our knowledge, this active compound is the most potent in vitro hTP inhibitor with a kinetic profile that cannot be reversed by the accumulation of any enzyme substrates.

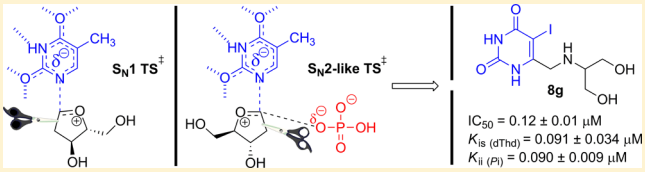

INTRODUCTION

Cancer is one of the leading causes of death worldwide, being responsible for approximately one in six deaths. According to the World Health Organization, the disease will claim 9.6 million lives in 2018, being the second leading cause of death globally.[1] Although cancer diagnosis and treatment have improved in the last few decades, providing a significant increase in patient survival rates, the clinical outcome of the disease remains clearly suboptimal with high rates of recurrence, invasiveness, and metastases. Ideally, new therapeutic strategies should act at different and critical stages of tumor progression to improve efficacy. Within this context, angiogenesis has emerged as a hallmark process in cancer growth and metastasis.[2] Since the early 1970s, it has been hypothesized that blocking angiogenesis could be a strategy to contain the disease's progress.[3] Since then, a large number of compounds targeting angiogenesis pathways have been under preclinical development, with many molecules currently in clinical trials or already approved for clinical use by the U.S. Food and Drug Administration (FDA).[4] Among the several factors that trigger vascular growth, human thymidine phosphorylase (hTP) stands out, as it has been described as a validated target for the development of antiangiogenic compounds.[5,6]

hTP is an enzyme involved in the pyrimidine salvage pathway, ensuring the reestablishment of pyrimidine nucleotides required for DNA repair and replication.[7] This enzyme catalyzes the reversible phosphorolysis of thymidine (dThd) in the presence of inorganic phosphates, yielding thymine and 2-deoxy-α-D-ribose-1-phosphate (2DDR-1P). Moreover, hTP shows deoxyribosyl transferase activity, by which the deoxyribosyl moiety is transferred from a pyrimidine nucleoside to a different pyrimidine base, generating the formation of

Received: August 17, 2018
Published: January 7, 2019

DOI: 10.1021/acs.jmedchem.8b01305
J. Med. Chem. 2019, 62, 1231−1245

new pyrimidine nucleosides.[8,9] Particularly, hTP has been described to possess an identical amino acid sequence to platelet-derived endothelial-cell growth factor (PD-ECGF) and gliostatin, indicating that they are the same proteins. PD-ECGF has been described to stimulate angiogenesis, while gliostatin is involved in the control of glial cell proliferation.[10−12]

hTP seems to play a pivotal role in the pathogenesis of cancer; unlike in healthy human tissues, its expression is upregulated in different types of tumors. In general, microenvironments of stressing conditions, such as hypoxia and low pH, tissues submitted to radio- and chemotherapy conditions, and the presence of different inflammatory cytokines, have resulted in increased levels of the enzyme.[6,13] Elevated levels of hTP are associated with cancer aggressiveness and poor prognosis, mainly due to the proangiogenic and antiapoptotic functions.[14−16]

The protumor signaling mechanism has been related to one of the products of the enzymatic reaction catalyzed by hTP. The cleavage of *N*-glycosidic bond leads to 2DDR-1P, which is converted to 2-deoxy-D-ribose (2DDR) by nonenzymatic dephosphorylation. Once outside the cell, 2DDR triggers angiogenic and antiapoptotic activities.[17−19] This molecule affects endothelial-cell migration by activation of the integrin downstream signaling pathway. Moreover, the augmented expression and/or secretion of other different angiogenic factors, such as interleukins, vascular endothelial growth factor (VEGF), and matrix metalloproteases, in the tumor microenvironment improves angiogenesis and cancer metastasis.[20−22] Furthermore, hTP and 2DDR have been correlated with protection against apoptosis in different types of tumor cells by hypoxia induction. Either hTP or 2DDR inhibited hypoxia-induced proapoptotic signals via several mechanisms, such as the activation of caspase-3 and caspase-9, mitochondrial transmembrane potential reduction, Bcl2 and Bcl-x_L down-regulation, mitochondrial cytochrome-*c* release, and HIF-1α upregulation.[16,23−25]

Aiming to suppress the angiogenic activity and apoptosis protection in tumor cells, different inhibitors of hTP have been designed as potential anticancer agents. Pyrimidine- and purine-based compounds, such as 6-amino-5-bromouracil (**1**) and 7-deazaxanthine (**2**), have been reported as inhibitors of thymidine phosphorylase (TP) activity (Figure 1).[26−28] It is

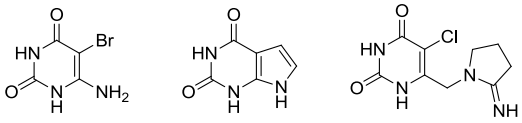

Figure 1. Chemical structures and IC_{50} of some pyrimidine- and purine-based inhibitors of hTP-catalyzed reactions.

important to mention that several inhibitors have been developed using *Escherichia coli* TP as a study model but their inhibitory profile on the human orthologous enzyme still needs to be analyzed. In 2015, the FDA approved the clinical use of Lonsurf, a combination of 5-chloro-6-[1-(2-iminopyrrolidinyl)methyl] (TPI; **3**), an hTP inhibitor, and trifluorothymidine, a chemotherapeutic agent, for the treatment of metastatic colorectal cancer (Figure 1).[29,30] TPI has been described as a competitive inhibitor of hTP-catalyzed reactions with an IC_{50} of 0.035 μM and a K_i of 0.020 μM.[29]

In an attempt to develop new hTP inhibitors that could hopefully be effective in the pathogenesis of cancer, the present study reports the design and synthesis of novel pyrimidine-based compounds. The molecules were designed to be analogous to the hTP transition state. Additionally, inhibition studies with the characterization of kinetic mechanisms for the most potent molecule and evaluation of the interaction mode using molecular docking were performed. Finally, early toxicity experiments, pharmacokinetic study, and the effect on xenograft tumor growth in vivo for the most effective hTP inhibitor are also shown.

RESULTS AND DISCUSSION

Design and Synthesis. The strategy for obtaining new compounds with inhibitory capacity on hTP was carried out in three distinct phases: (i) the synthesis of analogues to the transition state of the activated complex produced in the enzymatic catalysis, (ii) the choice of halogens as substituents on the 5-position of the heterocyclic ring uracil, and (iii) the use of different amino alcohols, mimicking 2DDR in an acyclic form.

Obtaining compounds analogous to the transition states of enzymatically catalyzed reactions has led to the development of the most potent inhibitors to date.[31,32] The hTP-catalyzed reaction is considered, from a chemical point of view, a nucleophilic substitution reaction that can be of first or second order (S_N1 or S_N2, respectively) (Figure 2). Two studies have described that thymidine arsenolysis catalyzed by hTP presents a concerted S_N2 mechanism.[33,34] The first proposed mechanism was symmetrical, with the nucleophile (arsenate) and the leaving group (thymine) showing approximately the same binding order.[33] In this study, a histidine-tagged protein was used that could modify the interpretation of the results.[34] An other work corroborated the S_N2-concerted mechanism; however, it was demonstrated that the transition state presents a carbocationic character with the likely formation of the ribooxocarbenium ion.[34] This fact was explained by the different orders of binding between the 1-*N*-ribosidic bond (C−N = 2.45 Å) and the distance of the arsenate relative to 2DDR (C−O = 2.95 Å) approaching the opposite side. On the other hand, it has been proposed that the hydrolysis of thymidine catalyzed by hTP undergoes an S_N1 transition state with the formation of a ribooxocarbonium intermediate without the participation of the nucleophile.[35] In this mechanism, the determinant step of the reaction speed was the nucleophilic attack of the water to the reaction intermediate. It is noteworthy that lack of inhibitory activity of the compounds geometrically and electronically similar to the S_N2 transition state has supported a transition state with a ribocationic character.[36] Therefore, herein, the objective was to synthesize compounds that could take advantage of the carbocation character presented by both the S_N1 and S_N2-like transition states proposed for hTP (Figure 2).

The second round was the choice of halogen at the 5-position of the heterocyclic uracil ring, substituting the methyl present at that position in the thymidine. Many compounds described as hTP inhibitors include chlorine (Cl), bromine (Br), or fluorine (F) attached to the 5-position of the above heterocyclic ring.[37−40] It is noteworthy that the high electronegativity of the halogenated substituents increases polarization of the heterocyclic ring, stabilizing the possible

DOI: 10.1021/acs.jmedchem.8b01305
J. Med. Chem. 2019, 62, 1231−1245

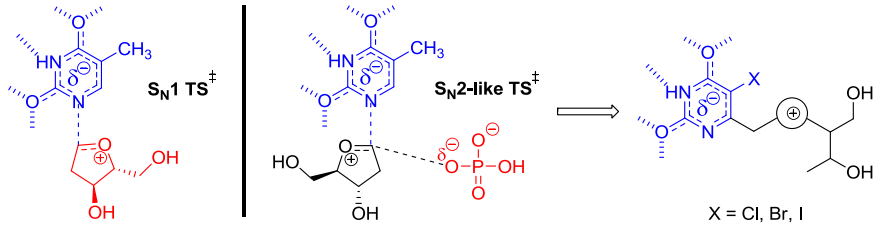

Figure 2. S_N1- and S_N2-like transition states proposed for the hTP-catalyzed reaction. Compounds were designed using amino groups on the side chain to allow the formation of a positively charged center similar to oxocarbenium formed at the transition state of the enzymatic reaction. The amino alcohols were used to mimic the open form of 2-deoxy-D-ribose attached to thymidine.

Scheme 1. Reactants and Conditions: i = DMF, 25−100 °C, 1 h; ii = H_2O, 25−35 °C, 6−20 h; iii = K_2CO_3, DMF, 25 °C, 16−18 h[a,b,c]

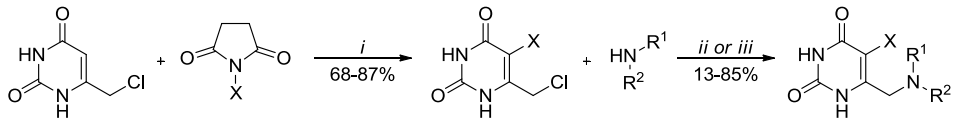

Entry	X	Yield (%)
6a	Cl	71
6b	Br	68
6c	I	87

Entry	X	R^1	R^2	Yield (%)[a]	Yield (%)[b]	IC$_{50}$ (μM)[c]
8a	Cl	H	CH_2CH_2OH	13	28	39 ± 5
8b	Cl	H	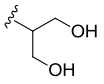	33	45	1.0 ± 0.2
8c	Br	H	CH_2CH_2OH	32	49	24 ± 2
8d	Br	H	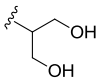	23	52	5.6 ± 0.9
8e	Br	H	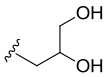	20	47	>100
8f	I	H	CH_2CH_2OH	21	45	1.2 ± 0.1
8g	I	H	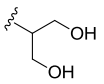	75	77	0.12 ± 0.01
8h	I	H	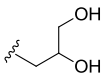	26	57	40 ± 7
8i	I	Me	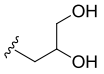	42	58	36 ± 7
8j	I	Me	Me	75	79	8.4 ± 0.5
8k	I	Pr	Pr	27	55	>100
8l	I	$CH_2(CH_2)_3CH_2$		21	46	28 ± 5
8m	I	$CH_2CH_2OCH_2CH_2$		71	76	87 ± 12
8n	I	H		77	85	34 ± 4

[a]Procedure ii. [b]Procedure iii. [c]Inhibitory activity of pyrimidine-2,4-diones **8a−n** over hTP-catalyzed reactions.

negative charge formed on the uracil ring similar to the transition states of hTP (S_N1 or S_N2-like mechanism). Nevertheless, this polarization reduces the pK_a of the heterocycle as it stabilizes its conjugate base. With increasing acidity, the hydrogen-bonding donor group as 3-NH forms more effective interactions, allowing greater stabilization of the complex through the presence of more efficient hydrogen bonds at the active site of the protein. Furthermore, the

DOI: 10.1021/acs.jmedchem.8b01305
J. Med. Chem. 2019, 62, 1231−1245

presence of halogens could establish halogens bonding with electron density donor groups through their σ hole.[41]

Finally, similar to that which has already been described,[42,43] the use of acyclic amino alcohols can mimic the oxocarbenium formed in the transition state catalyzed by hTP (Figure 2). This strategy of molecular simplification has already been shown to be efficient for maintaining inhibitory efficiency and facilitating chemical synthesis. The pK_a of the side chain (NH) of the amino alcohols can produce a positively charged center at physiological pH, similar to the oxocarbenium formed in the transition state for hTP.

The compounds were synthesized in two chemically simple steps from 6-(chloromethyl)-pyrimidine-2,4-(1*H*,3*H*)-dione (**4**). The first step was carried out from the reaction of compound **4** with the corresponding *N*-halosuccinimide **5** in the presence of dimethylformamide (DMF) as a solvent (Scheme 1). The halogenated product **6a**−**c** was obtained in yields of 68−87%. The second step was performed from the S_N2 nucleophilic substitution reaction of compound **6a**−**c** using amino alcohols or secondary amines (**7**). Two synthetic procedures were used to obtain the desired products (Scheme 1). The first method used water as solvent according to techniques already reported.[37,38] This environmental benign protocol furnished **8a**−**n** after reaction times of 6−20 h with yields ranging from 13 to 77%. The low yield obtained for some molecules was consistent with similar procedures previously described.[37,38] The second method employed DMF as solvent in the presence of potassium carbonate (K_2CO_3) as base. The reactants were stirred for 16−18 h, furnishing products with 28−85% yields. All compounds showed spectroscopy and spectrometric data consistent with the proposed structures (main text and Supporting Information).

In Vitro Inhibition Studies of hTP. The IC_{50} screening was employed to assess the relative potency of compounds against hTP activity and select the best compound for further studies.

The synthesized compounds **8a**−**n** inhibited the hTP activity with IC_{50} values ranging from 0.12 to 87 μM (Scheme 1). The inhibitory activity of compounds varied widely according to the different halogens at the 5-position of the heterocyclic ring and according to the substituents at R^1 and R^2. Of the two compounds having the Cl as halogen substituent at the 5-position of the uracil ring, compound **8b** was 39-fold more effective than compound **8a**. The same trend was observed for bromo-containing compounds. Indeed, molecule **8d** inhibited the enzymatic activity of hTP with a potency that was nearly 4-fold greater than that of **8c**. This denotes the importance of the insertion of a second hydroxyl in the side chain of compounds **8** as the ethanolamine derivatives (**8a** and **8c**) were less effective as inhibitors of hTP than compounds derived from 2-aminopropane-1,3-diol (**8b** and **8d**). This second hydroxyl formed, according to docking simulations (see the next section), a donor−acceptor pair of hydrogen bonds with hTP, which should be related to the better activity of these compounds.

The greatest inhibitory effect was observed for iodine-containing compounds at the 5-position of the uracil ring. It is interesting to note that iodine better positioned the structure **8g** at the active site of hTP than chlorine and bromine derivatives **8b** and **8d** according to docking findings. In addition, iodine was the halogen with the higher molecular volume and polarizability used in the series of synthesized compounds. These properties may be related to the better effectiveness of the inhibitory action, providing a better fit with the enzyme catalytic site and better stabilization of negative charge on the heterocyclic ring. Furthermore, iodine presents the largest σ hole among the halogens evaluated.[41] Thus, compounds containing this atom could perform halogen bond interactions more effectively. Once more, substitution using a 2-aminopropane-1,3-diol derivative (**8g**) led to the compound having the greatest inhibitory effect over hTP-catalyzed reactions. Structure **8g** showed an inhibitory effect that was 10-fold higher than that of **8f** (derived from ethanolamine). This second hydroxyl formed, according to docking simulations (see the next section), a donor−acceptor pair of hydrogen bonds with hTP, which should be related to the better activity elicited by the 2-aminopropane-1,3-diol derivatives **8b**, **8d**, and **8g**. By contrast, the presence of the 3-aminopropane-1,2-diol substituent in R^2 considerably decreased the inhibitory activity, leading to pyrimidine-2,4-dione **8h**, which exhibited an IC_{50} of 40 ± 7 μM (Scheme 1). An unexpected finding was presented by compound **8e**, which was inactive at a concentration of 100 μM. Compared with compounds **8d** and **8g**, this structural modification, by repositioning the hydroxyl from position β to position γ, considering the nitrogen, reduced the inhibition capacity of the enzyme by more than 300-fold. It was apparent from experiments that the position of a second hydroxyl exerts a significant effect on stabilizing the interaction of the inhibitor with the protein.

To increase the structural space of the compound series studied, the **8i**−**n** derivatives containing cyclic and acyclic alkyl groups in R^2 were synthesized. In these compounds, the iodine atom was maintained at the 5-position of the heterocyclic ring as it performed the best activity when compared to chlorine and bromine. None of these tested compounds exhibited a better inhibitory effectiveness on reactions catalyzed by the hTP enzyme than compound **8g** (Scheme 1). The apparent steric effect exerted by compound **8k** compared to its counterpart **8g** should be noted. Changing the dimethyl to dipropyl substituent abolished the inhibitory effectiveness since the **8k** compound did not exert any action when tested at a concentration of 100 μM, whereas **8j** inhibited the enzymatic activity of hTP with an IC_{50} of 8.4 ± 0.5 μM. On the basis of the inhibition data, compound **8g** was selected as the lead of this series of molecules and used in subsequent assays.

Prior to assessing the mode of inhibition of the most active compound, it was confirmed that its inhibitory activity is not time dependent up to 40 min of preincubation with hTP (data not shown). The mode of inhibition of pyrimidine-2,4-dione **8g** on the phosphorolysis activity, during the conversion of thymidine (dThd) nucleoside into thymine, was deduced by Lineweaver−Burk plots. The reciprocal of the rate of reaction was plotted against the reciprocal of substrate concentration, and the effect of inhibitor on both K_m and V_{max} was monitored. The in vitro inhibition constant values (K_{ii} and K_{is}) were determined by plotting the slope of each line in the Lineweaver−Burk plots against the different concentrations of **8g** and data fitting to an appropriate equation (eq 2). The K_i of **8g** was determined for both substrates. When the inorganic phosphate substrate (P_i) was fixed at a nonsaturating concentration and dThd was varied in the presence of fixed-varying concentrations of compound **8g**, the double-reciprocal plots gave a family of lines that intercept on the left of the y axis (Figure 3A). These results indicated that compound **8g**

DOI: 10.1021/acs.jmedchem.8b01305
J. Med. Chem. 2019, 62, 1231−1245

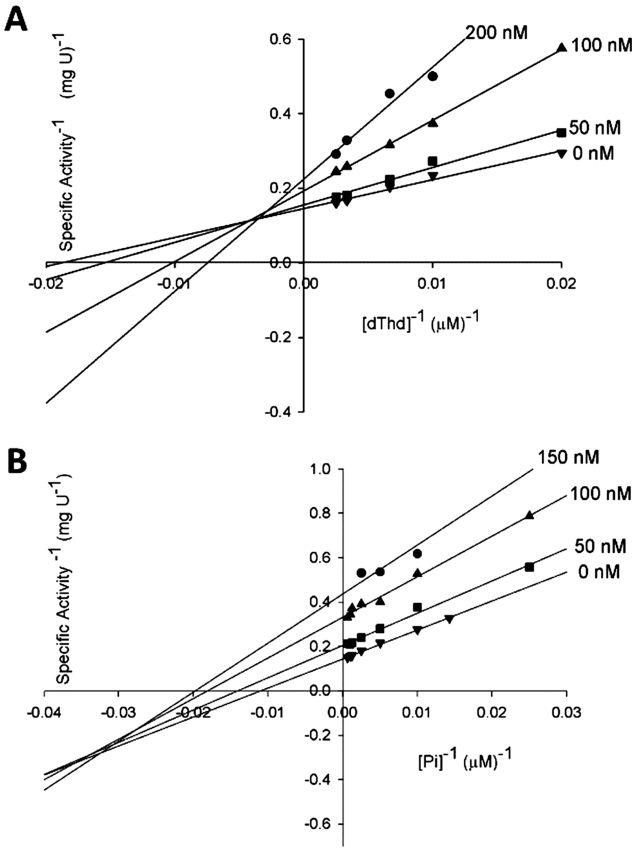

Figure 3. Determination of HTP-inhibition mechanism for compound **8g**. The Lineweaver–Burk plot displays a pattern of intersection to the left of the *y* axis toward dThd (A) and P_i (B), which is diagnostic of noncompetitive inhibition.

inhibited hTP in a noncompetitive manner with respect to dThd. Moreover, the analysis of the kinetic constants showed that the V_{max} of the enzyme decreased, whereas the K_m increased in the presence of increasing concentrations of compound **8g**, which is a typical effect of a noncompetitive inhibitor with $K_{is} < K_{ii}$.[44] This analysis was consistent with K_{is} and K_{ii} values obtained when fitting the data to eq 2, yielding K_{is} of 0.091 ± 0.034 μM and K_{ii} = 0.291 ± 0.88 μM. The inhibitory profile suggests that compound **8g** displays binding affinity for both the free enzyme (or enzyme–P_i binary complex) and the enzyme–P_i–dThd ternary complex; however, the inhibitor preferentially binds to the free enzyme. It is important to mention that the noncompetitive inhibition elicited for **8g** does not invalidate the design of the compound as a possible transition state analogue inhibitor, since the observed inhibition mode does not exclude that this molecule can interact at the dThd binding site.[44] Likewise, when P_i was the varied substrate in the presence of nonsaturating concentrations of dThd, compound **8g** also displayed a noncompetitive mode of inhibition, as indicated on the double-reciprocal plots (Figure 3B). Fitting data to eq 2 yielded a K_{is} value of 0.200 ± 0.114 μM and a K_{ii} value of 0.090 ± 0.009 μM. Compound **8g** exhibited $K_{is} > K_{ii}$, indicating a binding preference for the enzyme–dThd–P_i ternary complex in comparison to binding to either free enzyme or enzyme–dThd binary complex. In addition, the presence of increasing concentrations of inhibitor decreased both V_{max} and K_m, which reflected, once more, a noncompetitive signature with $K_{is} > K_{ii}$. Interestingly, a rapid-equilibrium random bi–bi kinetic mechanism has been proposed for hTP, in which both substrates can bind to a free enzyme to form the catalytically competent ternary complex; also, both products can randomly dissociate to yield free enzymes.[45] Compound **8g** inhibited the enzyme reaction in a noncompetitive fashion with respect to both dThd and P_i, in which the inhibitor can bind not only to the enzyme–substrate complex but also to the free enzyme without obeying

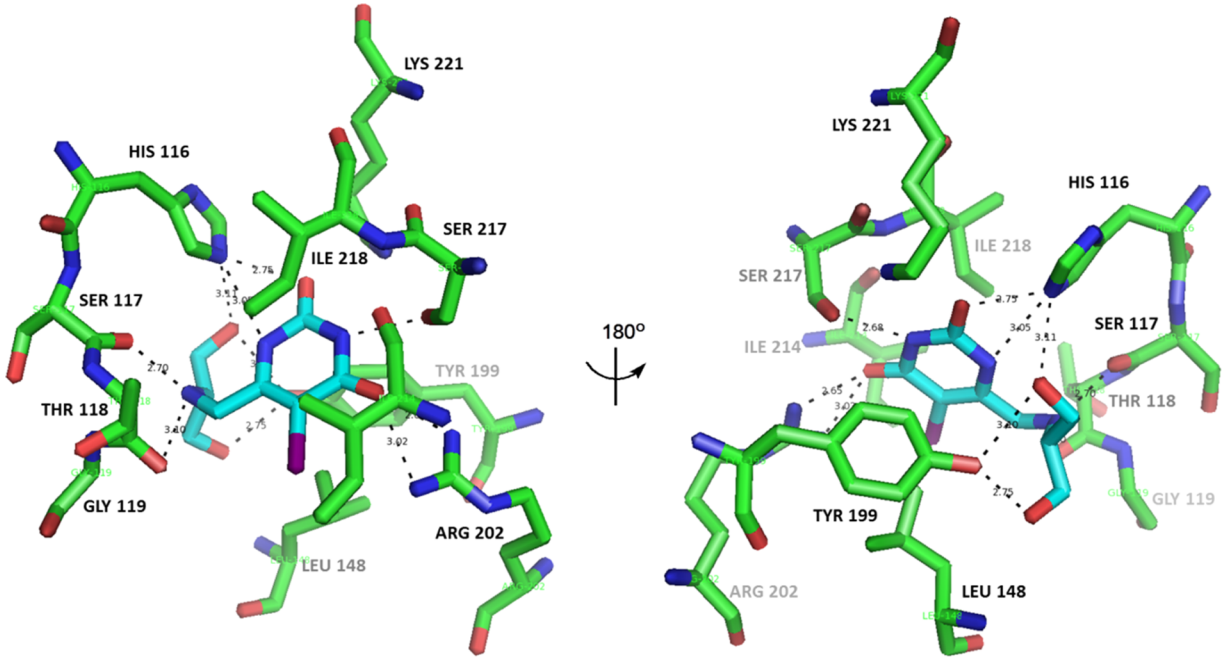

Figure 4. Binding mode of compound **8g** at active site of hTP (PDB: 2WK6) using Gold 5.5 molecular software. Graphic visualization obtained using PyMOL (v.0.99).

DOI: 10.1021/acs.jmedchem.8b01305
J. Med. Chem. 2019, 62, 1231–1245

a binding order, which is in agreement with the random bi−bi kinetic mechanism proposed for hTP.

Molecular Docking Studies. Docking studies were carried out to try to determine the key intermolecular interactions that occur upon enzyme−inhibitor complex formation. In addition, these assessments sought further evidence of the interaction site of synthesized pyrimidine-2,4-diones into hTP as noncompetitive inhibition mode presented by lead compound **8g** may generate some doubt. Simulations were performed with free enzyme using the coordinate obtained from the crystal structure of the hTP−5-iodouracil complex (protein data bank (PDB): 2WK6).[46] Docking using free enzyme allowed direct comparison with the interaction mode performed by 5-iodouracil, a simplified analogue of compound **8g**, at the active site of hTP.

Experiments showed that compound **8g** is stabilized at the hTP binding site through interactions with residues His116, Ser117, Thr118, Leu148, Tyr199, Arg202, Ser217, Ile218, and Lys221 (Figure 4). Incidentally, the residues His116, Arg202, Ser217, and Lys221, which stabilized the heterocyclic 5-iodouracil at the **8g** binary complex, are the same as those which make strong contacts at hTP−5-iodouracil cocrystal structure.[46] Carbonyl groups at the 2- and 4-position of **8g** act as hydrogen bond acceptors from Lys221, Arg202, and His116. The distances for acceptor−donor pairs were obtained with 3.02 and 2.65 Å for Arg202, 2.66 Å for Lys221, and 2.75 Å for His116 from carbonyl groups. Another hydrogen bond of the heterocyclic ring at the active site of hTP was observed between 3-NH and Ser217 with a distance of 2.68 Å. The 1-NH of uracil ring also established hydrogen bond contact with imidazole from His116 at a distance of 3.05 Å. Considering the side chain of compound **8g**, hydrogen bonds and van der Waals interactions were obtained between the 1,3-dihydroxypropanylamino group and amino acid residues Ser117, Thr118, and Tyr199. Amino group formed hydrogen bonds between the amino alcohol side chain and the active site of hTP using the backbone of Ser117 and Thr118 residues. Amino donor group was positioned 2.70 and 3.10 Å from Ser117 and Thr118, respectively. In addition, hydrogen bonds between the 4-hydroxy group of Tyr199 and the hydroxyl group of **8g** were observed with distance of 2.75 and 3.10 Å. Importantly, Tyr199 does not appear in the crystallographic studies among the amino acids that stabilize the 5-iodouracil or TPI at the catalytic site of hTP.[46,47] This difference may be related to the mode of enzymatic inhibition presented by structure **8g** when compared with TPI. One of these hydroxyl groups of the side chain of **8g** that acts as a hydrogen acceptor upon binding to Tyr199 participated as a hydrogen bond donor at distance of 3.11 Å from the donor group (τ-NH) present at His116. The intermolecular interactions of the two hydroxyl groups of the 1,3-dihydroxypropanylamino system depicted by docking experiments explain, in theory, the better hTP-inhibition profile of pyrimidine-2,4-diones **8b**, **8d**, and **8g** in comparison with molecules **8a**, **8c**, and **8f**, which contain ethanolamine as a side chain. Interestingly, the molecular docking was able to predict the best potency presented by compound **8g**. The best pose of molecules **8b**, **8d**, and **8g** showed an affinity energy of −80.2, −83.3, and −99.8 kcal/mol, respectively. Unlike **8b** and **8d**, iodine-containing compound **8g** positioned the amino alcohol side chain in a position that allowed strong interactions with Tyr199 and Thr118 (Supporting Information).

Early Toxicity and in Vitro Metabolic Stability Investigations. The cytotoxicity of hTP inhibitor **8g** on normal and tumor cells was evaluated using both 3-(4,5-dimethylthiazol-2-yl)-2,5-diphenyl-2*H*-tetrazolium bromide (MTT) and neutral red uptake (NRU) methods to assess cell viability. The MTT assay is able to evaluate the functional integrity of mitochondria on the basis of the ability for the enzymatic reduction of tetrazolium salt MTT by mitochondrial dehydrogenases to formazan crystal by living cells.[48] The NRU assay is based on the accumulation of the dye in the lysosome of viable cells.[49] The in vitro incubation with various concentrations of pyrimidine-2,4-dione **8g** (25, 50, 100, 250, and 500 μM) did not significantly affect the viability of HepG2, Vero, HaCat, RAW 264.7, and U-87 MG cells (Table 1). Only at the highest concentration evaluated (1000 μM), **8g** caused a statistically significant decrease in cell viabilities for all lineages evaluated using both MTT and NRU methodologies (Table 1).

To estimate genotoxicity, the induction of DNA single- and double-strand breaks and alkali-labile sites in HepG2 cells was evaluated using the alkaline comet assay. Results showed that the lead compound **8g** did not cause DNA-strand breaks, even at the highest concentration tested of 1000 μM (Figure 5). These results indicate a likely safety profile for **8g** on the basis of cytotoxic and genotoxic evaluations.

It is noteworthy that the viability of the glioblastoma cell line U-87 MG was evaluated in the presence of 25, 50, 100, 250, 500, and 1000 μM of pyrimidine-2,4-dione **8g**. In the experimental conditions tested, **8g** did not affect the in vitro cellular viability of U-87 MG. Afterward, in vitro drug−drug interactions were determined for compound **8g**. As angiogenesis inhibitors have been used as adjuvants in cancer chemotherapy, knowing the potential drug−drug interactions is crucial in early drug discovery. The drug−drug interactions were evaluated by assaying compound **8g** against a panel of human CYP450 isoforms (3A4, 1A2, 2C9, 2C19, 2D6, and 2E1). The results denoted a reduced risk of drug−drug interactions as the IC_{50} of the compound was >100 μM for all of the above isoforms (Supporting Information). Finally, in vitro intrinsic clearance analysis using human S9 fraction revealed that pyrimidine-2,4-dione **8g** exhibits moderate rates of metabolism with Cl_{int} of 13.0 mL/(min kg) and half-life of 28.1 min (Supporting Information).

Pharmacokinetics and in Vivo Antitumor Activity. Glioblastoma multiforme (GBM) is the most common and aggressive primary brain tumor among adults, with an average survival of approximately 15 months.[50,51] The standard protocol available for the treatment of GBM consists of maximal safe surgical resection, followed by radiotherapy, plus concomitant and adjuvant chemotherapy with the alkylating agent temozolamide (TMZ).[52,53] However, at least 50% of TMZ-treated patients do not respond to this agent. Moreover, hematological malignancies such as acute lymphoblastic leukemia, acute myeloid leukemia and myelodysplastic syndrome have been reported to occur after treatment with TMZ.[53−55]

Importantly, hTP is overexpressed in GBM, whereas undetectable or trace levels are found in the normal human brain.[56−58] The occurrences of microvascular proliferation, invasion, and resistance to apoptosis are hallmarks of glioblastoma.[58,59] Antiangiogenic therapy is considered an important target for GBM treatment, and several clinical trials enrolling antiangiogenic agents are in progress.[52,60−62] The

DOI: 10.1021/acs.jmedchem.8b01305
J. Med. Chem. 2019, 62, 1231−1245

Table 1. Effects of hTP Inhibitor 8g on HepG2, Vero, HaCat, RAW 264.7, and U-87 MG Cell Viabilities[a]

	% of cell viability ± SEM											
	HepG2		Vero		HaCat		RAW 264.7		U-87 MG	
compound concentration (μM)	MTT	NRU	MTT	NRU	MTT	NRU	MTT	NRU	MTT	NRU
25	103 ± 5	102 ± 5	101 ± 5	108 ± 3	105 ± 5	100 ± 4	103 ± 1	105 ± 2	101 ± 1	99 ± 3
50	100 ± 3	103 ± 3	97 ± 4	112 ± 1	95 ± 4	110 ± 2	99 ± 2	102 ± 2	97 ± 1	101 ± 3
100	100 ± 2	102 ± 4	96 ± 5	108 ± 3	98 ± 3	104 ± 3	99 ± 2	97 ± 3	96 ± 7	104 ± 4
250	100 ± 4	98 ± 4	95 ± 3	103 ± 1	96 ± 4	100 ± 6	95 ± 1	85 ± 3	97 ± 3	98 ± 3
500	94 ± 6	96 ± 3	84 ± 3	90 ± 4	93 ± 3	95 ± 4	91 ± 1	82 ± 9	89 ± 3	93 ± 8
1000	82 ± 6*	81 ± 7*	75 ± 3**	72 ± 5***	81 ± 4**	75 ± 7**	72 ± 7***	48 ± 14***	83 ± 3**	72 ± 7***

[a]Cells were incubated with treatments for 72 h, and cell viability was assessed by MTT or NRU assays. Data were expressed as the means of cell viability ± standard error of the means of three to five independent experiments performed in triplicate; untreated wells were considered to show 100% viability. Statistical analysis was performed by one-way analysis of variance (ANOVA) followed by Dunnett's multiple comparison test. Significances (compared to control group): * $p < 0.05$, ** $p < 0.01$, and *** $p < 0.001$.

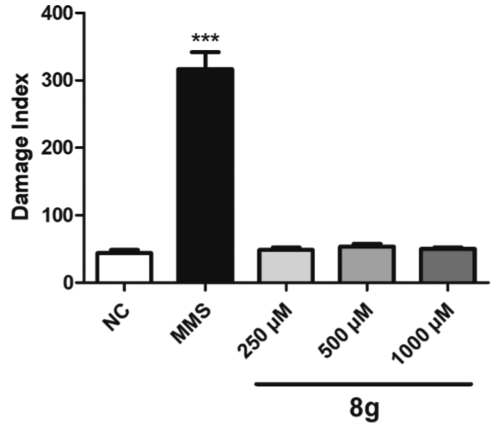

Figure 5. Induction of DNA damage measured with the alkaline comet assay in HepG2 cells incubated with pyrimidine-2,4-dione **8g**. NC = control group; methyl methanesulfonate (MMS) = positive control group. Results are expressed as a damage index and represent the mean ± standard error of the mean for three independent experiments. Statistical analysis was performed by one-way analysis of variance followed by Dunnett's multiple comparison test. Data significant in relation to control group at *** $p < 0.001$.

novel strategies for GBM treatment are focused on the modulation of vessel permeability, hypoxia, and tumor-induced edema.[54,58,60]

Pharmacokinetic studies were performed in mice after intraperitoneal (IP) administration of **8g** (50 mg/kg) (Table 2). Maximum plasma concentration (C_{max}) of 34.8 μg/mL was achieved after 0.08 h (T_{max}). The data corroborated the in vitro metabolic stability, indicating a rapid/moderate elimination rate with elimination rate constant (K_e) and elimination half-life ($t_{1/2}$) values of 1.38 h^{-1} and 0.5 h, respectively. In addition, the area under the concentration−time plot ($AUC_{0\rightarrow t}$ and $AUC_{0\rightarrow\infty}$) revealed a promising profile with values of 16.9 and 17.4 μg h/L, respectively. The obtained pharmacokinetic data supported subsequent in vivo effectiveness assays.

Table 2. Pharmacokinetic Parameters Determined after Intraperitoneal (IP) Administration of 8g (50 mg/kg) to Mice (Noncompartmental Analysis)[a]

parameters	50 mg/kg IP (n = 21)
C_{max} (μg/mL)	34.8
T_{max} (h)	0.08
K_e (h^{-1})	1.38
$t_{1/2}$ (h)	0.5
$AUC_{0\rightarrow t}$ (μg h/L)	16.9
$AUC_{0\rightarrow\infty}$ (μg h/L)	17.4
$AUMC_{0\rightarrow t}$ (μg h^2/L)	6.3
$AUMC_{0\rightarrow\infty}$ (μg h^2/L)	7.6
MRT (h)	0.4

[a]C_{max}: peak concentration; T_{max}: time to peak plasma concentration; K_e: elimination rate constant; $t_{1/2}$: elimination half-life; AUC: area under the concentration−time curve from 0 to time t; $AUC_{0\rightarrow\infty}$: area under the plasma concentration−time curve from time zero to infinity; $AUMC_{0\rightarrow t}$: area under the first moment of the plasma concentration−time curve; $AUMC_{0\rightarrow\infty}$: area under the first moment of the plasma concentration−time curve extrapolated to infinity; MRT: mean residence time; (n = 3 animals/sampling time point).

To evaluate the in vivo antitumoral activity of the lead compound **8g**, human GBM tumor cells (U-87 MG) were

DOI: 10.1021/acs.jmedchem.8b01305
J. Med. Chem. 2019, 62, 1231−1245

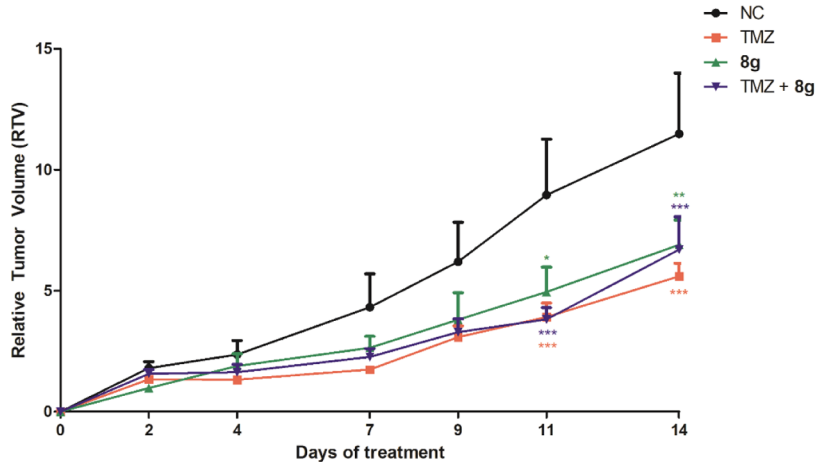

Figure 6. Effects of lead compound **8g** on the relative tumor volume (RTV) of U-87 MG human glioblastoma tumor implanted into the right flank of nude mice. NC = vehicle-treated group; TMZ = temozolamide. Statistical analysis was performed by a two-way analysis of variance followed by Bonferroni post-tests. Data significant in relation to control group at * $p < 0.05$, ** $p < 0.01$, and *** $p < 0.001$.

subcutaneously injected into the flank of nude mice. After tumors reached a volume of approximately 50 mm^3, the animals were randomly divided and received intraperitoneal administrations of NaCl 0.9% (control group), the compound **8g**, TMZ, or a combination of TMZ plus **8g**, for 14 days. The results revealed a significant decrease of tumor growth in mice treated with pyrimidine-2,4-dione **8g**, TMZ, or with the combination of both, when compared with the control group (Figure 6). The reduction of tumor growth rate started after 11 days of treatment, and it was maintained until euthanasia (14 days treatment). Importantly, tumor-bearing nude mice treated with **8g** did not show significant body weight alterations whereas animals receiving TMZ showed a slight decrease (less than 20% body weight change (BWC)) in body weight. These observations indicate that both **8g** alone or in combination may not cause important toxic effects (Supporting Information).

Immunohistochemistry (IHC) and histological analysis supported the capacity of the compound **8g** to act on tumor angiogenesis, by reducing the immunolabeling for VEGF, the major angiogenic factor present in GBM,[56] and CD31, a marker of vascular endothelium.[63] In addition, **8g** was able to reduce the density of blood vessels present in the tumor tissue, compared to that in the control group (Figure 7). The antitumor activity of the combined therapy was not statistically different when compared to the treatment with TMZ alone. Moreover, we have observed reduced VEGF staining and number of vessels in the group treated with the combination TMZ and **8g**. The TMZ group, even having a reduced tumor growth, did not show any difference in the histochemical analysis, when compared to the control group (Figure 7). The immunostaining for Ki-67 (cell proliferation marker), or capase-3 (the apoptosis marker) was not significantly different among the experimental groups (Supporting Information). The low total percentage of apoptotic tumor cells present in U-87 MG cells could partially explain our outcome for caspase-3 labeling;[64] however, further studies are needed to clarify this point. Moreover, the lack of efficacy of our compound in the proliferation of tumor cells demonstrated by Ki-67 staining is in agreement with the in vitro results (Table 1), as the pyrimidine-2,4-dione **8g** was inactive against U-87 MG cell.[65]

CONCLUSIONS

Herein, we have designed and synthesized potent inhibitors of human thymidine phosphorylase (hTP). The design was based on the possible oxocarbenium character of the transition state proposed for enzyme-catalyzed phosphorolysis. In addition, the synthetic process involved simple and easily accessible reagents and reactants. The most potent compound was able to inhibit the enzyme with IC_{50} and K_i in the submicromolar range with a noncompetitive inhibition mode with respect to both substrates (thymidine and inorganic phosphate). To the best of our knowledge, this is, to date, the most potent inhibitor of hTP, with an inhibition mechanism that cannot be reversed by the accumulation of both substrates (thymidine and inorganic phosphate). Competitive inhibition results in building up of substrate concentrations that can overcome the inhibitor effect and ensuing increase in enzyme activity. Unlike competitive inhibitors, noncompetitive inhibitors cannot be overcome by high concentrations of a substrate as the inhibitor can bind to enzyme−substrate complexes and decrease enzyme activity. Moreover, the most effective compound exhibited low cytotoxicity against HepG2, Vero, HaCat, RAW 264.7, and U-87 MG lineages, absence of genotoxicity in the alkaline comet assay, low probability of drug−drug interactions accessed through CYP450 inhibition studies, and moderate in vitro metabolic rates. Finally, in a model of glioblastoma cancer xenografts, the lead compound **8g** was able to significantly reduce tumor growth when administered to nude mice. The reduction in tumor volume growth was comparable to that presented by temozolomide, a first-line drug for glioblastoma multiforme treatment. These results demonstrate that this class of compounds may provide drug candidates for the treatment of various solid cancers, targeting angiogenesis, the anti-apoptotic activity stimulated by hTP, and/or its role in fluoropyrimidine-based therapy. Additionally, the overexpression of hTP is involved in a variety of pathological complications, such as psoriasis, atherosclerosis, rheumatoid arthritis, inflammatory bowel disease, and mitochondrial neurogastrointestinal encephalomyopathy. In diseases such as these, hTP inhibitors can play an important role and, hopefully, bring about an improvement in the patients' quality of life.

DOI: 10.1021/acs.jmedchem.8b01305
J. Med. Chem. 2019, 62, 1231−1245

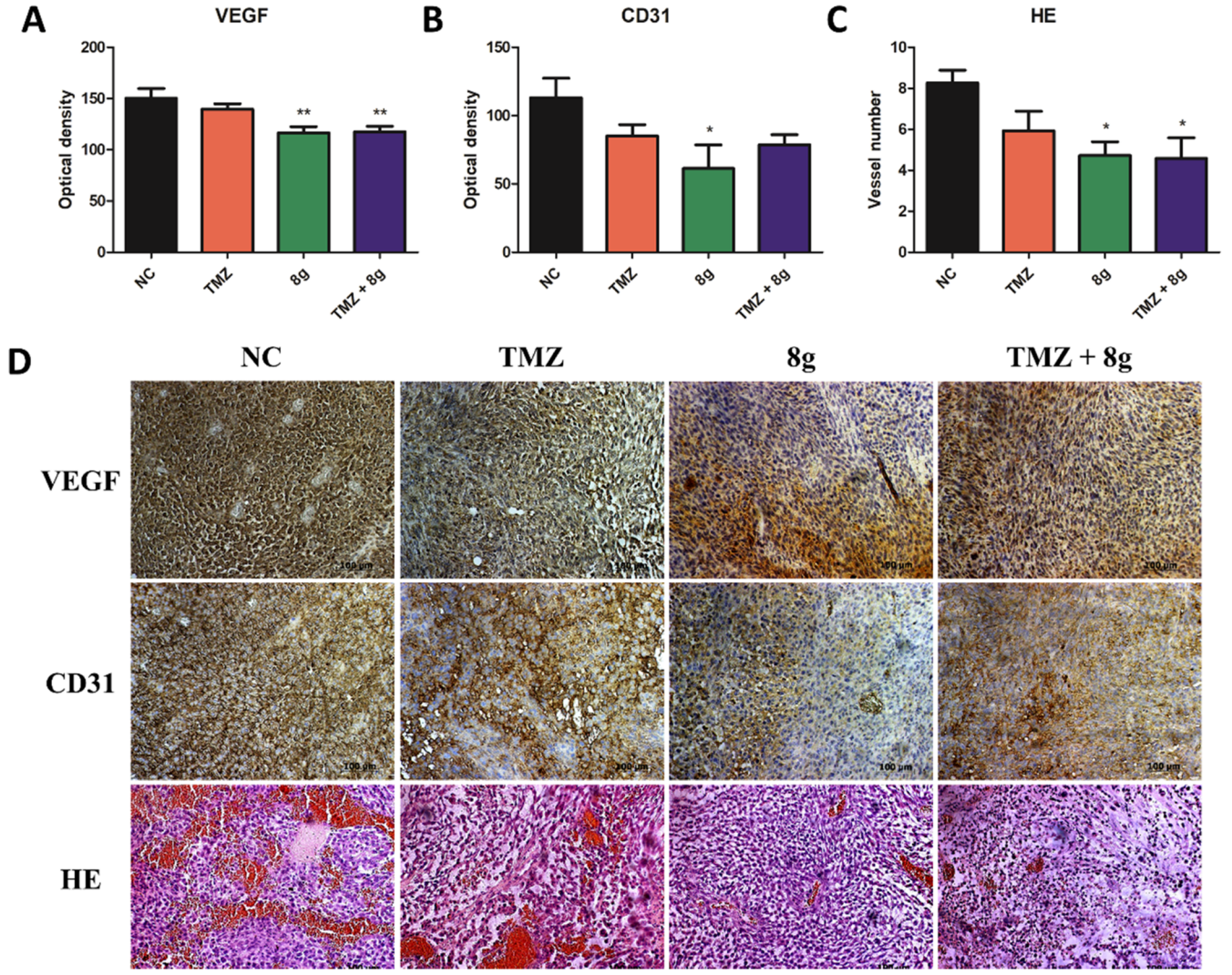

Figure 7. Immunohistochemistry and histological analysis. Mean of positive areas of immunolabeling for (A) VEGF (angiogenesis marker), (B) CD31 (vascular endothelium marker), and (C) number of blood vessels present in the tumor tissue, compared to control group. (D) Representative images of IHC labeling of VEGF, CD31, and hematoxylin−eosin (HE) staining in different treatment groups. NC = control group; TMZ = temozolamide. Results are expressed as optical density or number of vessels and represent the mean ± standard error of the mean for four images captured per tumor (×200). Statistical analysis was performed by one-way analysis of variance followed by Dunnett's multiple comparison test. Data significant in relation to control group at * $p < 0.05$ and ** $p < 0.01$.

EXPERIMENTAL SECTION

Chemistry and Structure: Apparatus and Analysis. The commercially available reactants and solvents were obtained from commercial suppliers and were used without any purification. The reactions were monitored by thin-layer chromatography (TLC) with Merck TLC silica gel 60 F_{254}. The melting points were measured using a Microquímica MQAPF-302 apparatus. ^{1}H and ^{13}C NMR spectra were acquired on a Anasazi EFT-60 (^{1}H NMR at 60.13 MHz) or Avance III HD Bruker (^{13}C NMR at 400.13 MHz) spectrometer. Chemical shifts (δ) were expressed in parts per million relative to dimethyl sulfoxide (DMSO)-d_6, which was used as the solvent, and to tetramethylsilane, which was used as an internal standard. High-resolution mass spectra (HRMS) were obtained for all of the compounds on an LTQ Orbitrap Discovery mass spectrometer (Thermo Fisher Scientific, Bremer, Germany). This system combines an LTQ XL linear ion-trap mass spectrometer and an Orbitrap mass analyzer. The analyses were performed through the direct infusion of the sample in MeOH/H_2O (1:1) with 0.1% formic acid (flow rate 10 μL/min) in a positive-ion mode using electrospray ionization (ESI). For elemental composition, calculations used the specific tool included in the Qual Browser module of Xcalibur (Thermo Fisher Scientific, release 2.0.7) software. Compound purity was determined using an Äkta high-performance liquid chromatography (HPLC) system (GE Healthcare Life Sciences) equipped with a binary pump, manual injector, and UV detector. Unicorn 5.31 software (Build 743) was used for data acquisition and processing. The HPLC conditions were as follows: RP column 5 μm Nucleodur C-18 (250 × 4.6 mm^2); flow rate 1.5 mL/min; UV detection 254 nm; and 100% water (1% acetic acid) maintained from 0 to 7 min, followed by a linear gradient from 100% water (1% acetic acid) to 90% acetonitrile/methanol (1:1, v/v) from 7 to 15 min (15−30 min) and subsequently returned to 100% water (1% acetic acid) in 5 min (30−35 min) and maintained for an additional 10 min (35−45 min). All of the evaluated compounds were ≥95% pure.

General Procedure for the Synthesis of 6-(Chloromethyl)-5-halopyrimidine-2,4(1*H*,3*H*)-diones 6. Selected Example for Compound 6-(Chloromethyl)-5-iodopyrimidine-2,4(1*H*,3*H*)-dione (6c). To a solution of 6-(chloromethyl)pyrimidine-2,4-(1*H*,3*H*)-dione (**4**) (1.606 g, 10 mmol) in DMF (15 mL), *N*-iodosuccinimide (**5c**) (2.475 g, 11 mmol) in DMF (5 mL) was added. The mixture was stirred at 25 °C until the complete addition of **5c**. Thereafter, the temperature was raised to 100 °C and the reaction mixture was stirred for 1 h. The resultant solution was added on ice

DOI: 10.1021/acs.jmedchem.8b01305
J. Med. Chem. 2019, 62, 1231−1245

for precipitation. Afterward, the amorphous solid formed was filtered off and washed with cold water (3 × 15 mL). Finally, the product was dried under reduced pressure for at least 48 h to give 2.492 g (87%) of **6c** as a white powder in good purity. Melting point: 226−227 °C. HPLC 95.0% (t_R = 12.86 min). ^{1}H NMR (60 MHz, DMSO-d_6): δ 4.51 (s, 2H, CH_2), 11.56 (br s, 2H). ^{13}C NMR (100 MHz, DMSO-d_6): δ 32.1 (CH_2), 58.4 (C-5), 149.4 (C-2), 158.3 (C-6), 160.8 (C-4). Fourier transform infrared (FT-IR) (UATR, cm^{-1}): 3136, 2970, 2825, 1645, 1427, 1312, 1078, 877, 687. HRMS (ESI) calcd for $C_5H_4ClIN_2O_2$ + H, 286.9079; found, 286.9071 $(M + H)^+$.

General Procedure for the Synthesis of 6-(Aminomethyl)-pyrimidine-2,4(1*H*,3*H*)-dione 8. Selected Example for Compound 6-(((1,3-Dihydroxypropan-2-yl)amino)methyl)-5-iodo-pyrimidine-2,4(1*H*,3*H*)-dione (8g). (Procedure ii) The mixture of 6-(chloromethyl)-5-iodopyrimidine-2,4(1*H*,3*H*)-dione (**6c**) (5.0 mmol, 1.432 g) and 2-aminopropane-1,3-diol (15.0 mmol, 1.366 g) in water (15 mL) was stirred at 35 °C for 20 h. The solid obtained was washed with water (3 × 15 mL), cold diethyl ether (10 mL), and NaOH 1% (10 mL, v/v). Finally, the product was crystallized from methanol and subsequently dried under reduced pressure to give 1.279 g (75%) of **8g** as white powder. Melting point: 164−167 °C. HPLC 98.6% (t_R = 12.80 min). ^{1}H NMR (60 MHz, DMSO-d_6): δ 2.47 (quint, 1H, CH), 3.38 (d, 4H, $2CH_2$), 3.69 (s, 2H, CH_2), 6.82 (br s, 2H). ^{13}C NMR (100 MHz, DMSO-d_6): δ 51.4 (CH_2), 60.8 (C-5), 61.1 ($2CH_2$), 68.1 (CH), 150.1 (C-2), 155.8 (C-6), 161.2 (C-4). FT-IR (UATR, cm^{-1}): 3138, 3003, 2817, 1655, 1605, 1427, 1079, 878. HRMS (ESI) calcd for $C_8H_{12}IN_3O_4$ + H, 341.9945; found, 341.9916 $(M + H)^+$.

(Procedure iii) 6-(Chloromethyl)-5-iodopyrimidine-2,4(1*H*,3*H*)-dione (**6c**) (1.0 mmol, 0.286 g) was diluted in *N*,*N*-dimethylformamide (5 mL) with the addition of potassium carbonate (K_2CO_3, 2.0 mmol) and 2-aminopropane-1,3-diol (2.0 mmol, 0.182 g) under an argon atmosphere at 25 °C. The reaction mixture was stirred for 18 h, and the precipitated product filtered off, washed with water (3 × 15 mL), cold diethyl ether (10 mL), and NaOH 1% (10 mL, v/v). Finally, the product was crystallized from methanol and subsequently dried under reduced pressure to give 0.220 g (77%) of **8g** as white powder. HPLC 97.3% (t_R = 12.82 min). ^{1}H NMR and HRMS were consistent with the proposed structure and above presented data.

In Vitro Enzyme Inhibition Studies. The recombinant HTP was expressed and purified to homogeneity and had its enzymatic activity assayed, as previously described.[45] To assess the relative potency of the compounds, inhibition studies were performed by steady-state kinetic studies using a UV-2550 UV/visible spectrophotometer (Shimadzu), monitoring a decrease in the change in absorbance upon the conversion of thymidine (dThd) to thymine at 290 nm (ε_{dThd} = 2000 M^{-1} cm^{-1}) for 1 min. Experiments were performed at 37 °C in 50 mM Tris buffer pH 7.4, and measurement of the enzyme-catalyzed reaction started with the addition of 10 μL of hTP at 2 μM to the assay mixture in a final volume of 500 μL. The preliminary screening to evaluate the inhibitory activity of a set of compounds was performed through the determination of IC_{50} values. The IC_{50} values, which define the concentration of inhibitor necessary to achieve 50% inhibition of the reaction velocity,[44] were determined by adding different concentrations of the compounds (dissolved in DMSO or water) to the reaction mixture. The maximal rate of the enzymatic reaction was determined in the absence of inhibitor and in the presence of fixed nonsaturating concentrations of dThd ($K_m \cong 70$ μM) and phosphate (P_i) ($K_m \cong 110$ μM),[45] in the presence or absence of 1% DMSO. The reaction velocity was analyzed as the percentage of inhibition as a function of inhibitor concentration, and IC_{50} values were estimated using eq 1

$$\frac{v_i}{v_0} = \frac{1}{1 + \frac{[I]}{IC_{50}}} \quad (1)$$

The most promising compound **8g** (dissolved in water) was further evaluated to deduce the mechanism of inhibition and to determine the inhibition constants (K_i). A potential inhibitor may interact with an enzyme in a competitive, noncompetitive, or uncompetitive manner if inhibition follows a rapid-equilibrium mode. Prior to assessing the inhibition profile, it is necessary to ascertain whether inhibition is not time dependent or if there is a slow step for the equilibrium process. Accordingly, recombinant hTP was preincubated with 50 nM inhibitor (final concentration) and aliquots were taken at different times (up to 40 min) and added to the reaction mixture, as previously described. The change in initial velocity as a function of time was monitored, and the percent inhibition was determined.

Lineweaver−Burk (double-reciprocal) plots were used to determine the mode of inhibition, and data fitting to appropriate equation gave values for the inhibition constants (K_{is} and/or K_{ii}). The inhibition studies were carried out for dThd and P_i substrate analysis at varying concentrations of inhibitor. Initial rates were measured as a function of dThd concentrations (50−500 μM) at a fixed nonsaturating P_i concentration (110 μM) and fixed-varied inhibitor concentrations (50, 100, and 150 nM); for P_i, initial rates were measured as a function of P_i concentrations (70−1600 μM) at a fixed nonsaturating dThd concentration (70 μM) and fixed-varied inhibitor concentrations (50, 100, and 150 nM). The K_i values toward dThd and P_i were estimated using eq 2, which describes a noncompetitive inhibition, where [I] is the inhibitor concentration, [S] is the substrate concentration, K_m and V_{max} are the Michaelis−Menten constant and maximum velocity, respectively, K_{ii} is the overall inhibition constant for the enzyme−substrate−inhibitor complex, and K_{is} is the overall inhibition constant for the enzyme−inhibitor complex. The diagnostic signature of noncompetitive inhibition displays a nest of lines that intersect at a point other than the *y* axis in a double-reciprocal plot.[44] All initial velocity measurements for each substrate concentration were performed in duplicate.

$$v_0 = \frac{V_{max}[S]}{K_m\left(1 + \frac{[I]}{K_{is}}\right) + [S]\left(1 + \frac{[I]}{K_{ii}}\right)} \quad (2)$$

Molecular Docking Studies. Computational studies were performed with pyrimidine-2,4-diones **8b**, **8d**, and **8g**. DFT B3LYP/6-311G* basis in gas-phase methodology, evaluable in Spartan'08 for Windows software (Wavefunction Inc., Irvine), was used for geometric optimization and conformational analysis by submitting to a systematic search, with torsion angle increases set to 30° in the range 0−360°. The lowest energy conformer for chemical structure was saved in mol2 files before use in docking studies.

The structure of hTP, encoded PDB ID: 2WK6,[46] was downloaded from the protein data bank (PDB) before performing docking studies; this three-dimensional structure was prepared by the removal of water molecules and the addition of polar hydrogens using the Autodock Tools 1.5.6.[66] Molecular docking studies were performed using iGemdock 2.1[67] and Gold 5.5 software[68,69] in which the individual binding poses of a compound were assessed and submitted to docking in the active site of the 2WK6. Igemdock docking calculations were performed at the drug screening docking accuracy setting with GA parameters set for population size, generation, and number of solutions as 200, 70, and 3, respectively, and a Gemdock score function of hydrophobic and electrostatic (1:1 preference). Residue consensus analysis was used as post screening analysis to improve screening accuracy of calculated results. The iGemdock software was used to infer the intermolecular interactions between the enzyme active site and the compound studied.

A genetic algorithm using an automatic search with an efficiency of 100% and range from 100 to 12 500 operations, as implemented in GOLD 5.5, was applied to calculate the 10 possible conformations of the compound that may bind to the protein. Default parameters, such as a population size of 100, selection pressure (1.1), number of islands of 1, niche size 2, operator weights for migration 0, mutate and crossover 100, were also applied. The GOLD scoring function used was the ChemPLP.

Cell-Based Assays. *Cell Culture and Treatments.* Human keratinocyte (HaCat), African green monkey kidney epithelium (Vero), murine macrophage (RAW 264.7), human hepatocellular carcinoma (HepG2), and human glioblastoma (U-87 MG) immortalized cell lines were cultured under standard conditions in

DOI: 10.1021/acs.jmedchem.8b01305
J. Med. Chem. 2019, 62, 1231−1245

Dulbecco's modified Eagle's medium (Invitrogen) supplemented with 10% heat-inactivated fetal bovine serum (Invitrogen), 1% penicillin–streptomycin (Invitrogen), and 0.1% fungizone (Invitrogen). Cells were kept in tissue-culture flasks at 37 °C in a humidified atmosphere containing 5% CO_2.

For the 3-(4,5-dimethylthiazol-2-yl)-2,5-diphenyl-2*H*-tetrazolium bromide (MTT, Sigma) assay and neutral red uptake (NRU) assay, HaCat, Vero, HepG2, and U-87 MG cells were seeded at 2×10^3 cells/well, and RAW 264.7 cells at 5×10^2 cells in a 96-well culture plate and incubated for 24 h to adhere. Compound **8g**, at concentrations varying from 25 to 1000 μM, was then incubated with cells for 72 h. For the comet assay, HepG2 cells were seeded at 5×10^4 cells/well in a 24-well culture plate for 24 h before treatment with **8g** at concentrations of 250, 500, and 1000 μM for additional 24 h.

MTT Assay. MTT was performed according to an already described protocol.[70] Briefly, after incubation for 72 h at 37 °C under 5% CO_2, the cultures were incubated with MTT solution (1 mg/mL) for 3 h. The formazan crystals were dried at room temperature for 24 h and then dissolved with 100 μL of DMSO. The absorbance was measured at 595 nm (SpectraMax M2e, Molecular Devices). The mean absorbance of negative control wells was set as 100% viability, and the values of treated cells were calculated as the percentage of control.

NRU Assay. After cell incubation for 72 h at 37 °C under 5% CO_2, the NRU assay was performed according to Borenfreund and Puerner.[71] Cells were washed with phosphate-buffered saline (PBS), and then 200 μL of neutral red dye solution (25 μg/mL, Sigma) prepared in serum-free medium was added to the plate and incubated for 3 h at 37 °C under 5% CO_2. Cells were washed with PBS before the addition of 100 μL of a desorb solution (ethanol/acetic acid/water, 50:1:49), followed by gentle shaking for 30 min, for dye dissolution. Cell viability was expressed as a percentage considering the untreated control cell as 100%.

Comet Assay. The alkaline comet assay was performed by using a previously reported method[72] with minor modifications. After 24 h of incubation with compound **8g**, 60 μL of HepG2 suspension (1×10^4) was mixed with 180 μL of low-melting point agarose and spread on microscope slides precoated with regular agarose and placed at 4 °C for 10 min for total agarose solidification. Cells were lysed in ice-cold solution (2.5 M NaCl, 100 mM Na_2EDTA, 10 mM Tris with 1% Triton X-100, and 10% DMSO) for 24 h. Therefore, the slides containing the cells were washed with PBS and then exposed to alkali conditions (300 mM NaOH, 1 mM ethylenedinitrilotetraacetic acid, pH > 13) at 4 °C for 20 min, to allow DNA unwinding and the expression of alkali-labile sites. Electrophoresis was conducted for 20 min at 25 V and 300 mA. Subsequently, the slides were neutralized, fixed, and stained using silver nitrate staining. Methyl methanesulfonate (MMS) at 100 μM was used as positive control group.[73] One hundred cells from each slide were visually scored according to the size and amount of DNA present in the tail. Separately, each cell was given an arbitrary value of 0 (undamaged) to 4 (maximum damage).[74] The damage score was thus attributed to each slide and ranged from 0 (undamaged: 100 cells × 0) to 400 (maximum damage: 100 cells × 4).

Pharmacokinetic Study. Twenty-one male CF1 mice were used for the intraperitoneal (IP) injection of **8g**. The animals were divided in seven groups, each containing three animals/time point. A single injection (50 mg/kg) of the compound (dissolved in 0.9% saline solution) was administered, and the animals were euthanized 0.03, 0.08, 0.25, 0.5, 1, and 2 h after dosing. The blood samples were collected into heparin tubes (BD Vacutainer).

Noncompartmental analysis was performed to determine the pharmacokinetic parameters. The maximum concentration of drug in plasma (C_{max}) and time to C_{max} (T_{max}) were directly obtained from graphs of the concentration versus time curve. The area under the concentration–time curve from 0 min to the last experimental point 2 h ($AUC_{0\to t}$) and the area under the first moment of the plasma concentration–time curve ($AUMC_{0\to t}$) were calculated by the trapezoidal rule. The elimination rate constant (K_e) was estimated by linear regression taking into account the last concentrations (Ln *C*/time profile). The total area from time zero from infinity ($AUC_{0\to\infty}$) was calculated by $AUC_{0\to\infty} = AUC_{0\to t} + C_{last}/K_e$, where C_{last} is the last measured concentration. The AUMC was extrapolated to infinity by $AUMC_{0\to\infty} = AUMC_{0\to t} + C_{last}. t_{last}/K_e + C_{las}/K_e^2$, where t_{last} is the last measured time. The half-life ($t_{1/2}$) was calculated by the equation $t_{1/2} = 0.693/K_e$. Finally, the mean residence time (MRT) was obtained with the equation ($AUMC_{0\to\infty}/AUC_{0\to\infty}$).[75,76] This protocol was previously approved by the local Animal Ethics Committee (CEUA/PUCRS, protocol number: 8731/2018).

In Vivo Antitumor Activity. Male BALB/c nude mice were obtained from Instituto Lauro de Souza Lima (Bauru, Brazil) and were housed in groups of four per cage. They were maintained at a controlled temperature (24 ± 2 °C) and humidity (60–70%), under a 12 h light–dark cycle, with food and water available ad libitum. For the subcutaneous tumor xenograft model, 5×10^5 U-87 MG cells were implanted into the right flank of nude mice.[77,78] The animals were randomly divided into four groups: Control (saline), temozolamide (TMZ, 50 mg/(kg day)),[79,80] pyrimidine-2,4-dione **8g** (50 mg/(kg day)), or a combination of TMZ (50 mg/(kg day)) plus **8g** (50 mg/(kg day)). When the mean tumor volume reached more than 50 mm^3 (day 0), the intraperitoneal treatments were started and given for 5 days/week for two cycles.

The tumor diameters were measured three times per week, and the tumor volume (*V*) was estimated as $V = 0.5 \times \text{length (mm)} \times \text{width}^2$ (mm). The individual relative tumor volume (RTV) was calculated by the formula: RTV = (tumor volume on the measured day)/(tumor volume on day 0). On day 14, the tumor growth-inhibition (TGI) ratio was calculated using the following formula: TGI = [1 − (RTV of the treated group)/(RTV of the control group)] × 100 (%). The body weight change (BWC) was calculated using the formula: BWC (%) = [(body weight on the last day) − (body weight on day 0)]/(body weight on day 0) × 100 (%). Body weight with a loss of above 20% or animal death during the treatment was considered to be indicative of toxicity.[81,82] These protocols were previously approved by the local Animal Ethics Committee (CEUA-PUCRS, protocol number: 8059/2017). We followed the ARRIVE Guidelines to report in vivo experiments.[83]

Immunohistochemistry and Histological Analysis. Following 14 days of treatment, the mice were euthanized and the tumors were collected and immediately fixed in 4% buffered formaldehyde solution, paraffin embedded, and sectioned into 3 μm slices for immunohistochemistry (IHC) and hematoxylin–eosin (HE) analysis. The technique for IHC was performed as previously described with some modifications.[84] High-temperature antigen recovery was performed by immersion of the slides in a water bath at 95–98 °C in 10 mM trisodium citrate buffer, pH 6, for 40 min. The peroxidase was blocked by incubation with 5% perhidrol for 30 min, and the nonspecific protein binding was blocked with 5% milk serum solution for 30 min. Polyclonal VEGF antibody (1:300, Cat. PA5-16754, Cat. SK2482305B, Thermo Fisher Scientific), monoclonal CD31 antibody (JC/70A) (1:100, Cat. MA5-13188, Lot. SK 2483693B, Thermo Fisher Scientific), monoclonal Ki-67 antibody (SP6) (1:300, Cat. MA5-14520, Lot. SK2478526A, Thermo Fisher Scientific), and monoclonal rabbit caspase-3 antibody (9H19L2) (1:150, Cat. 700182, Lot. SF256052, Thermo Fisher Scientific, Invitrogen Bioservices India) were used as primary antibodies by overnight incubation at 4 °C. The slides were washed with PBS and incubated with the secondary antibody horseradish peroxidase conjugate (ready-to-use, Dako Cytomation, Carpinteria, CA), for 20 min at room temperature. The slides were washed in PBS and were incubated with 3,3′-diaminobenzidine in chromogen solution (DAB + Chromogen, Dako Cytomation) and counterstained lightly with Harris's hematoxylin solution. Images were examined with a Zeiss AxioImager M2 light microscope (Carl Zeiss, Gottinge, Germany). The image capture was performed in ×200 (anti-caspase-3, anti-CD31 and anti-VEGF) or ×400 (anti-Ki-67) magnifications (four to six fields per slide), and they were evaluated by using the ImageJ 1.52e Software (NIH, Bethesda, MD). Since dark-to-medium brown regions

DOI: 10.1021/acs.jmedchem.8b01305
J. Med. Chem. 2019, 62, 1231–1245

represent the positivity antibody labeling, a specific macro was created to quantify the positive areas on the basis of optical density.[85]

For the HE analysis, the hot-spot technique was used to obtain the vessel densities. The mean vessel counts from four fields/tumor in ×200 magnifications were used. Areas of gross hemorrhage were avoided.[86]

Statistical Analysis. The in vitro cell assays and in vivo results were expressed as mean ± standard error of the mean, and statistical significance was determined by one-way analysis of variance (ANOVA) followed by Dunnett's multiple comparison test, except for RTV values, which were analyzed by two-way ANOVA followed by the Bonferroni post-test. The statistical software GraphPad Prism, version 5 (San Diego, CA) was used for all analyses, and $p < 0.05$ indicated statistical significance.

■ ASSOCIATED CONTENT

Supporting Information

The Supporting Information is available free of charge on the ACS Publications website at DOI: 10.1021/acs.jmedchem.8b01305.

Synthesis and characterization of compounds (^{1}H and ^{13}C NMR, FT-IR, and high-resolution mass spectrometry); intermolecular forces obtained from docking studies; metabolic drug−drug interaction assay; in vitro metabolic stability assay; HPLC analysis and sample preparation (pharmacokinetics); body weight change (BWC) after treatment with **8g**; immunohistochemistry and histological analysis (PDF)

Coordinate information for structure representation (PDB)

Molecular formula strings and some data (CSV)

■ AUTHOR INFORMATION

Corresponding Authors

*E-mail: luiz.basso@pucrs.br. Phone/Fax: +55 51 33203629 (L.A.B.).

*E-mail: pablo.machado@pucrs.br. Phone/Fax: +55 51 33203629 (P.M.).

ORCID

Sidnei Moura: 0000-0003-1903-6735

Luiz Augusto Basso: 0000-0003-0903-2407

Pablo Machado: 0000-0001-5616-9583

Author Contributions

○N.D.d.M.S. and C.D.R. contributed equally to this work.

Author Contributions

The manuscript was written through contributions of all authors. All authors have given approval to the final version of the manuscript.

Notes

The authors declare no competing financial interest.

■ ACKNOWLEDGMENTS

This work was supported by FAPERGS-PRONUPEQ (grant number: 16/2551-0000523-0), Banco Nacional de Desenvolvimento Econômico e Social (BNDES/FUNTEC) (grant number 14.2.0914.1) and National Institute of Science and Technology on Tuberculosis (Decit/SCTIE/MS-MCT-CNPq-FNDTC-CAPES-FAPERGS) (grant number 421703/2017-2). S.M., A.P.D.d.S., M.M.C, C.V.B., L.A.B., and P.M. are research career awardees of the CNPq. We thank Dr. Dejair Caitano do Nascimento from Instituto Lauro de Souza Lima for the kind donation of nude mice and Dr. Janaína Pasetti Nunes for her help with the experiments of immunohistochemistry.

■ ABBREVIATIONS

2DDR, 2-deoxy-D-ribose; 2DDR-1P, 2-deoxy-α-D-ribose-1-phosphate; ANOVA, one-way analysis of variance; AUC, area under the concentration−time curve from 0 to time t; $AUC_{0\rightarrow\infty}$, area under the plasma concentration−time curve from time zero to infinity; $AUMC_{0\rightarrow t}$, area under the first moment of the plasma concentration−time curve; $AUMC_{0\rightarrow\infty}$, area under the first moment of the plasma concentration−time curve extrapolated to infinity; BWC, body weight change; C_{max}, peak concentration; CYP, cytochrome P; DMF, dimethylformamide; DMSO, dimethyl sulfoxide; dThd, thymidine; ESI, electrospray ionization; FDA, U.S. Food and Drug Administration; GBM, glioblastoma multiforme; HPLC, high-performance liquid chromatography; HRMS, high-resolution mass spectra; hTP, human thymidine phosphorylase; IC_{50}, concentration of inhibitor that reduces enzyme velocity by half; K_e, elimination rate constant; K_i, inhibition constants; MMS, methyl methanesulfonate; MRT, mean residence time; MTT, (3-(4,5-dimethylthiazol-2-yl)-2,5-diphenyl-2*H*-tetrazolium bromide); NaCl, sodium chloride; NRU, neutral red uptake; PD-ECGF, platelet-derived endothelial-cell growth factor; P_i, inorganic phosphate substrate; RTV, relative tumor volume; $t_{1/2}$, elimination half-life; TLC, thin-layer chromatography; T_{max}, time to peak plasma concentration; TMZ, temozolomide; TPI, 5-chloro-6-[1-(2-iminopyrrolidinyl)-methyl]; VEGF, vascular endothelial growth factor

■ REFERENCES

(1) World Health Organization. *WHO Fact Sheets*, 2018. http://www.who.int/news-room/fact-sheets/detail/cancer (accessed Nov 16, 2018).

(2) Carmeliet, P.; Jain, R. K. Angiogenesis in Cancer and Other Diseases. *Nature* **2000**, *407*, 249−257.

(3) Folkman, J. Tumor Angiogenesis: Therapeutic Implications. *N. Engl. J. Med.* **1971**, *285*, 1182−1186.

(4) Cook, K. M.; Figg, W. D. Angiogenesis Inhibitors: Current Strategies and Future Prospects. *Ca-Cancer J. Clin.* **2010**, *60*, 222−243.

(5) Elamin, Y. Y.; Rafee, S.; Osman, N.; O'Byrne, K. J.; Gately, K. Thymidine Phosphorylase in Cancer; Enemy or Friend? *Cancer Microenviron.* **2016**, *9*, 33−43.

(6) Bera, H.; Chigurupati, S. Recent Discovery of Non-nucleobase Thymidine Phosphorylase Inhibitors Targeting Cancer. *Eur. J. Med. Chem.* **2016**, *124*, 992−1003.

(7) Friedkin, M.; Roberts, D. The Enzymatic Synthesis of Nucleosides. I. Thymidine Phosphorylase in Mammalian Tissue. *J. Biol. Chem.* **1954**, *20*, 254−256.

(8) Schwartz, M. Thymidine phosphorylase from *Escherichia coli*. Properties and kinetics. *Eur. J. Biochem.* **1971**, *21*, 191−198.

(9) Iltzsch, M. H.; El Kouni, M. H.; Cha, S. Kinetic Studies of Thymidine Phosphorylase from Mouse Liver. *Biochemistry* **1985**, *24*, 6799−6807.

(10) Moghaddam, A.; Bicknell, R. Expression of Platelet-derived Endothelial Cell Growth Factor in *Escherichia coli* and Confirmation of its Thymidine Phosphorylase Activity. *Biochemistry* **1992**, *31*, 12141−12146.

(11) Usuki, K.; Saras, J.; Waltenberger, J.; Miyazono, K.; Pierce, G.; Thomason, A.; Heldin, C. H. Platelet-derived Endothelial Cell Growth Factor has Thymidine Phosphorylase Activity. *Biochem. Biophys. Res. Commun.* **1992**, *184*, 1311−1316.

(12) Asai, K.; Nakanishi, K.; Isobe, I.; Eksioglu, Y. Z.; Hirano, A.; Hama, K.; Miyamoto, T.; Kato, T. Neurotrophic Action of Gliostatin on Cortical Neurons. Identity of Gliostatin and Platelet-derived

Endothelial Cell Growth Factor. *J. Biol. Chem.* **1992**, *267*, 20311−20316.
(13) Brown, N. S.; Jones, A.; Fujiyama, C.; Harris, A. L.; Bicknell, R. Thymidine Phosphorylase Induces Carcinoma Cell Oxidative Stress and Promotes Secretion of Angiogenic Factors. *Cancer Res.* **2000**, *60*, 6298−6302.
(14) Moghaddam, A.; Zhang, H. T.; Fan, T. P. D.; Hu, D. E.; Lees, V. C.; Turley, H.; Fox, S. B.; Gatter, K. C.; Harris, A. L.; Bicknell, R. Thymidine Phosphorylase is Angiogenic and Promotes Tumor Growth. *Proc. Natl. Acad. Sci. U.S.A.* **1995**, *92*, 998−1002.
(15) Matsuura, T.; Kuratate, I.; Teramachi, K.; Osaki, M.; Fukuda, Y.; Ito, H. Thymidine Phosphorylase Expression is Associated with Both Increase of Intratumoral Microvessels and Decrease of Apoptosis in Human Colorectal Carcinomas. *Cancer Res.* **1999**, *59*, 5037−5040.
(16) Ikeda, R.; Furukawa, T.; Mitsuo, R.; Noguchi, T.; Kitazono, M.; Okumura, H.; Sumizawa, T.; Haraguchi, M.; Che, X. F.; Uchimiya, H.; Nakajima, Y.; Ren, X. Q.; Oiso, S.; Inoue, I.; Yamada, K.; Akiyama, S. Thymidine Phosphorylase Inhibits Apoptosis Induced by Cisplatin. *Biochem. Biophys. Res. Commun.* **2003**, *301*, 358−363.
(17) Haraguchi, M.; Miyadera, K.; Uemura, K.; Sumizawa, T.; Furukawa, T.; Yamada, K.; Akiyama, S.; Yamada, Y. Angiogenic Activity of Enzymes. *Nature* **1994**, *368*, 198.
(18) Liekens, S.; Bilsen, F.; De Clercq, E.; Priego, E. M.; Camarasa, M. J.; Pérez-Pérez, M. J.; Balzarini, J. Antiangiogenic Activity of a Novel Multi-substrate Analogue Inhibitor of Thymidine Phosphorylase. *FEBS Lett.* **2002**, *510*, 83−88.
(19) Miyadera, K.; Sumizawa, T.; Haraguchi, M.; Yoshida, H.; Konstanty, W.; Yamada, Y.; Akiyama, S. Role of Thymidine Phosphorylase Activity in the Angiogenic Effect of Platelet Derived Endothelial Cell Growth Factor/Thymidine Phosphorylase. *Cancer Res.* **1995**, *55*, 1687−1690.
(20) Hotchkiss, K. A.; Ashton, A. W.; Klein, R. S.; Lenzi, M. L.; Zhu, G. H.; Schwartz, E. L. Mechanisms by Which Tumor Cells and Monocytes Expressing the Angiogenics Factor Thymidine Phosphorylase Mediate Human Endothelial Cell Migration. *Cancer Res.* **2003**, *63*, 527−533.
(21) Bijnsdorp, I. V.; Capriotti, F.; Kruyt, F. A.; Losekoot, N.; Fukushima, M.; Griffioen, A. W.; Thijssen, V. L.; Peters, G. J. Thymidine Phosphorylase in Cancer Cells Stimulates Human Endothelial Cell Migration and Invasion by the Secretion of Angiogenic Factors. *Br. J. Cancer* **2011**, *104*, 1185−1192.
(22) Tabata, S.; Yamamoto, Y.; Goto, H.; Hirayama, A.; Onishi, M.; Kuramoto, T.; Mitsuhashi, A.; Ikeda, T.; Haraguchi, M.; Kawahara, K.; Shinsato, Y.; Minami, K.; Saijo, A.; Hanibuchi, M.; Nishioka, K.; Sone, S.; Esumi, H.; Tomita, M.; Soga, T.; Furukawa, T.; Akiyama, S. Thymidine Catabolism as a Metabolic Strategy for Cancer Survival. *Cell Rep.* **2017**, *19*, 1313−1321.
(23) Ikeda, R.; Furukawa, T.; Kitazono, M.; Ishitsuka, K.; Okumura, H.; Tani, A.; Sumizawa, T.; Haragushi, M.; Komatsu, M.; Uchimiya, H.; Ren, X. Q.; Motoya, T.; Yamada, K.; Akayama, S. Molecular Basis for the Inhibition of Hypoxia-induced Apoptosis by 2-Deoxy-*D*-ribose. *Biochem. Biophys. Res. Commun.* **2002**, *291*, 806−812.
(24) Jeung, H. C.; Che, X. F.; Haraguchi, M.; Furukawa, T.; Zheng, C. L.; Sumizawa, T.; Rha, S. Y.; Roh, J. K.; Akiyama, S. Thymidine Phosphorylase Suppresses Apoptosis Induced by Microtubule-interfering Agents. *Biochem. Pharmacol.* **2005**, *70*, 13−21.
(25) Jeung, H. C.; Che, X. F.; Haraguchi, M.; Zhao, H. Y.; Furukawa, T.; Gotanda, T.; Zheng, C. L.; Tsuneyoshi, K.; Sumizawa, T.; Roh, J. K.; Akiyama, S. Protection Against DNA Damage Induced Apoptosis by the Angiogenic Factor Thymidine Phosphorylase. *FEBS Lett.* **2006**, *580*, 1294−1302.
(26) Langen, P.; Etzold, G.; Barwolff, D.; Preussel, B. Inhibition of Thymidine Phosphorylase by 6-Aminothymine and Derivatives of 6-Aminouracil. *Biochem. Pharmacol.* **1967**, *16*, 1833−1837.
(27) Balzarini, J.; Gamboa, A. E.; Esnouf, R.; Liekens, S.; Neyts, J.; De Clercq, E.; Camarasa, M. J.; Pérez-Pérez, M. J. 7-Deazaxanthine, a Novel Prototype Inhibitor of Thymidine Phosphorylase. *FEBS Lett.* **1998**, *438*, 91−95.
(28) Liekens, S.; Hernandez, A. I.; Ribatti, D.; De Clercq, E.; Camarasa, M. J.; Pérez-Pérez, M. J.; Balzarini, J. The Nucleoside Derivative 5′-*O*-Trityl-inosine (KIN59) Suppresses Thymidine Phosphorylase Triggered Angiogenesis via a Noncompetitive Mechanism of Action. *J. Biol. Chem.* **2004**, *279*, 29598−29605.
(29) Fukushima, M.; Suzuki, N.; Emura, T.; Yano, S.; Kazuno, H.; Tada, Y.; Yamada, Y.; Asao, T. Structure and Activity of Specific Inhibitors of Thymidine Phosphorylase to Potentiate the Function of Antitumor 2′-Deoxyribonucleosides. *Biochem. Pharmacol.* **2000**, *59*, 1227−1236.
(30) Emura, T.; Suzuki, N.; Fujioka, A.; Ohshimo, H.; Fukushima, M. Potentiation of the Antitumor Activity of Alpha, Alpha, Alpha-trifluorothymidine by the Coadministration of an Inhibitor of Thymidine Phosphorylase at a Suitable Molar Ratio in vivo. *Int. J. Oncol.* **2005**, *27*, 449−455.
(31) Schramm, V. L. Enzymatic Transition States: Thermodynamics, Dynamics and Analogue Design. *Arch. Biochem. Biophys.* **2005**, *433*, 13−26.
(32) Schramm, V. L. Transition States, analogues, and Drug Development. *ACS Chem. Biol.* **2013**, *8*, 71−81.
(33) Birck, M. R.; Schramm, V. L. Nucleophilic Participation in the Transition State for Human Thymidine Phosphorylase. *J. Am. Chem. Soc.* **2004**, *126*, 2447−2453.
(34) Schwartz, P. A.; Vetticatt, M. J.; Schramm, V. L. Transition State Analysis of the Arsenolytic Depyrimidination of Thymidine by Human Thymidine Phosphorylase. *Biochemistry* **2011**, *50*, 1412−1420.
(35) Schwartz, P. A.; Vetticatt, M. J.; Schramm, V. L. Transition State Analysis of Thymidine Hydrolysis by Human Thymidine Phosphorylase. *J. Am. Chem. Soc.* **2010**, *132*, 13425−13433.
(36) Evans, G. B.; Gainsford, G. J.; Schramm, V. L.; Tyler, P. C. The Synthesis of Possible Transition State Analogue Inhibitors of Thymidine Phosphorylase. *Tetrahedron Lett.* **2015**, *56*, 406−409.
(37) Yano, S.; Kazuno, H.; Suzuki, N.; Emura, T.; Wierzba, K.; Yamashita, J.; Tada, Y.; Yamada, Y.; Fukushima, M.; Asao, T. Synthesis and Evaluation of 6-Methylene-bridged Uracil Derivatives. Part 1: Discovery of Novel Orally Active Inhibitors of Human Thymidine Phosphorylase. *Bioorg. Med. Chem.* **2004**, *12*, 3431−3441.
(38) Yano, S.; Kazuno, H.; Sato, T.; Suzuki, N.; Emura, T.; Wierzba, K.; Yamashita, J.; Tada, Y.; Yamada, Y.; Fukushima, M.; Assao, T. Synthesis and Evaluation of 6-Methylene-bridged Uracil Derivatives. Part 2: Optimization of Inhibitors of Human Thymidine Phosphorylase and their Selectivity with Uridine Phosphorylase. *Bioorg. Med. Chem.* **2004**, *12*, 3443−3450.
(39) Pérez-Pérez, M. J.; Priego, E. V.; Hernández, A. I.; Camarasa, M. J.; Balzarini, J.; Liekens, S. Thymidine Phosphorylase Inhibitors: Recent Developments and Potential Therapeutic Applications. *Mini-Rev. Med. Chem.* **2005**, *5*, 1113−1123.
(40) Jain, H. V.; Rasheed, R.; Kalman, T. I. The Role of Phosphate in the Action of Thymidine Phosphorylase Inhibitors: Implications for the Catalytic Mechanism. *Bioorg. Med. Chem. Lett.* **2010**, *20*, 1648−1651.
(41) Clark, T.; Hennemann, M.; Murray, J. S.; Politzer, P. Halogen Bonding: The Sigma-hole. *J. Mol. Model.* **2007**, *13*, 291−296.
(42) Semeraro, T.; Lossani, A.; Botta, M.; Ghiron, C.; Alvarez, R.; Manetti, F.; Mugnaini, C.; Valensin, S.; Focher, F.; Corelli, F. Simplified Analogues of Immucillin-G Retain Potent Human Purine Nucleoside Phosphorylase Inhibitory Activity. *J. Med. Chem.* **2006**, *49*, 6037−6045.
(43) Clinch, K.; Evans, G. B.; Fröhlich, R. F.; Furneaux, R. H.; Kelly, P. M.; Legentil, L.; Murkin, A. S.; Li, L.; Schramm, V. L.; Tyler, P. C.; Woolhouse, A. D. Third-generation Immucillins: Syntheses and Bioactivities of Acyclic Immucillin Inhibitors of Human Purine Nucleoside Phosphorylase. *J. Med. Chem.* **2009**, *52*, 1126−1143.
(44) Copeland, R. A. Reversible Modes of Inhibitor Interactions with Enzymes. *Evaluation of Enzyme Inhibitors in Drug Discovery: a Guide for Medicinal Chemists and Pharmacologists*, 2nd ed.; John Wiley & Sons, Inc.: Hoboken, New Jersey, 2013; pp 48−80.

DOI: 10.1021/acs.jmedchem.8b01305
J. Med. Chem. 2019, 62, 1231−1245

(45) Deves, C.; Rostirolla, D. C.; Martinelli, L. K. B.; Bizarro, C. V.; Santos, D. S.; Basso, L. A. The Kinetic Mechanism of Human Thymidine Phosphorylase − a Molecular Target for Cancer Drug Development. *Mol. Biosyst.* **2014**, *10*, 592−604.
(46) Mitsiki, E.; Papageorgiou, A. C.; Iyer, S.; Thiyagarajan, N.; Prior, S. H.; Sleep, D.; Finnis, C.; Acharya, K. R. Structures of Native Human Thymidine Phosphorylase and in Complex with 5-Iodouracil. *Biochem. Biophys. Res. Commun.* **2009**, *386*, 666−670.
(47) Norman, R. A.; Barry, S. T.; Bate, M.; Breed, J.; Colls, J. G.; Ernill, R. J.; Luke, R. W. A.; Minshull, C. A.; McAlister, M. S. B.; McCall, E. J.; McMiken, H. H. J.; Paterson, D. S.; Timms, D.; Tucker, J. A.; Pauptit, R. A. Crystal Structure of Human Thymidine Phosphorylase in Complex with a Small Molecule Inhibitor. *Structure* **2004**, *12*, 75−84.
(48) van Meerloo, J.; Kaspers, G. J. L.; Cloos, J. Cell Sensitivity Assays: The MTT Assay. In Cancer Cell Culture. *Methods Mol. Biol.* **2011**, *731*, 237−245.
(49) Repetto, G.; del Peso, A.; Zurita, J. L. Neutral Red Uptake Assay for the Estimation of Cell Viability/Cytotoxicity. *Nat. Protoc.* **2008**, *3*, 1125−1131.
(50) Field, K. M.; Jorndan, J. T.; Wen, P. Y.; Rosenthal, M. A.; Reardon, D. A. Bevacizumab and Glioblastoma: Scientific Review, Newly Reported Updates, and Ongoing Controversies. *Cancer* **2015**, *121*, 997−1007.
(51) Kamiya-Matsuoka, C.; Gilbert, M. R. Treating Recurrent Glioblastoma: an Update. *CNS Oncol.* **2015**, *4*, 91−104.
(52) Batchelor, T. T.; Reardon, D. A.; Groot, J. F.; Wick, W.; Weller, M. Antiangiogenic Therapy for Glioblastoma: Current Status and Future Prospects. *Clin. Cancer Res.* **2014**, *20*, 5612−5619.
(53) Lee, S. Y. Temozolomide Resistance in Glioblastoma Multiforme. *Genes Dis.* **2016**, *3*, 198−210.
(54) Goyal, S.; Singh, R. R.; Balukrishna, S.; Bindra, M.; Bachianathan, S. An Early and Rare Second Malignancy in a Treated Glioblastoma Multiforme: Is it Radiation or Temozolomide? *J. Clin. Diagn. Res.* **2015**, *9*, 5−7.
(55) Momota, H.; Narita, Y.; Miyakita, Y.; Shibui, S. Secondary Hematological Malignancies Associated with Temozolomide in Patients with Glioma. *Neuro-Oncology* **2013**, *15*, 1445−1450.
(56) Takano, S.; Yamashita, T.; Ohneda, O. Molecular Therapeutic Targets for Glioma Angiogenesis. *J. Oncol.* **2010**, No. 351908.
(57) Blanquicett, C. G.; Gillespie, Y.; Nabors, L. B.; Miller, C. R.; Bharara, S.; Buchsbaum, D. J.; Diaso, R. B.; Johnson, M. R. Induction of Thymidine Phosphorylase in Both Irradiated and Shielded, Contralateral Human U87MG Glioma Xenografts: Implications for a Dual Modality Treatment Using Capecitabine and Irradiation. *Mol. Cancer. Ther.* **2002**, *1*, 1139−1145.
(58) Backos, D. S.; Fritz, K. S.; McArthur, D. G.; Kepa, J. K.; Donson, A. M.; Petersen, D. R.; Foreman, N. K.; Franklin, C. C.; Reigan, P. Glycation of Glutamate Cysteine Ligase by 2-Deoxy-*D*-ribose and its Potential Impact on Chemoresistance in Glioblastoma. *Neurochem. Res.* **2013**, *38*, 1838−1849.
(59) Noch, E.; Khalili, K. Molecular Mechanisms of Necrosis in Glioblastoma: The Role of Glutamate Excitotoxicity. *Cancer Biol. Ther.* **2009**, *8*, 1791−1797.
(60) Zhang, M.; Ye, G.; Li, J.; Wang, Y. Recent Advance in Molecular Angiogenesis in Glioblastoma: The Challenge and Hope for Anti-angiogenic Therapy. *Brain Tumor Pathol.* **2015**, *32*, 229−236.
(61) Torres, A.; Vargas, Y.; Uribe, D.; Carrasco, C.; Torres, C.; Rocha, R.; Oyarzún, C.; San Martín, R.; Quezada, C. Pro-apoptotic and Anti-angiogenic Properties of the α/β-Thujone Fraction from *Thuja occidentalis* on Glioblastoma Cells. *J. Neurooncol.* **2016**, *128*, 9−19.
(62) Kang, W.; Kin, S. H.; Cho, H. J.; Jin, J.; Lee, J.; Joo, K. M.; Nam, D. H. Talin1 Targeting Potentiates Anti-angiogenic Therapy by Attenuating Invasion and Stem-like Features of Glioblastoma Multiforme. *Oncotarget* **2015**, *6*, 27239−27251.
(63) Majchrzak, M.; Kaspera, W.; Szynusz, J.; Bobek-Billewicz, B.; Hebda, A.; Majchrzak, H. Markers of Angiogenesis (CD31, CD34, rCBV) and Their Prognostic Value in Low-grade Gliomas. *Neurol. Neurochir. Pol.* **2013**, *47*, 325−331.
(64) Martens, T.; Schmidt, N. O.; Eckerick, C.; Fillbrandt, R.; Merchant, M.; Schwall, R.; Westphal, M.; Lamszus, K. A Novel One-Armed Anti-c-Met Antibody Inhibits Glioblastoma Growth in vivo. *Clin. Cancer Res.* **2006**, *12*, 6144−6152.
(65) Babae, N.; Bourajjaj, M.; Liu, Y.; Beijnum, J. R. V.; Cerisoli, F.; Scaria, P. V.; Verheul, M.; Berkel, M. P. V.; Pieters, E. H. E.; Haastert, R. J. V.; Yousefi, A.; Mastrobattista, E.; Storm, G.; Berezikov, E.; Cuppen, E.; Woodle, M.; Schaapveld, R. Q. J.; Prevost, G. P.; Griffioen, A. W.; Noort, P. I. V.; Schiffelers, R. M. Systemic miRNA-7 Delivery Inhibits Tumor Angiogenesis and Growth in Murine Xenograft Glioblastoma. *Oncotarget* **2014**, *5*, 6687−6700.
(66) Morris, G. M.; Huey, R.; Lindstrom, W.; Sanner, M. F.; Belew, R. K.; Goodsell, D. S.; Olson, A. J. Autodock4 and AutoDockTools4: Automated Docking with Selective Receptor Flexibility. *J. Comput. Chem.* **2009**, *30*, 2785−2791.
(67) Yang, J. M.; Chen, C. C. GEMDOCK: A Generic Evolutionary Method for Molecular Docking. *Proteins: Struct., Funct., Bioinf.* **2004**, *55*, 288−304.
(68) Jones, G.; Willett, P.; Glen, R. C.; Leach, A. R.; Taylor, R. Development and Validation of a Genetic Algorithm for Flexible Docking. *J. Mol. Biol.* **1997**, *267*, 727−748.
(69) Verdonk, M. L.; Cole, J. C.; Hartshorn, M. J.; Murray, C. W.; Taylor, R. D. Improved Protein-Ligand Docking Using GOLD. *Proteins* **2003**, *52*, 609−623.
(70) Renck, D.; Machado, P.; Souto, A. A.; Rosado, L. A.; Erig, T.; Campos, M. M.; Farias, C. B.; Roesler, R.; Timmers, L. F. S. M.; Souza, O. N.; Santos, D. S.; Basso, L. A. Design of Novel Potent Inhibitors of Human Uridine Phosphorylase-1: Synthesis, Inhibition Studies, Thermodynamics, and in vitro Influence on 5-Fluorouracil Cytotoxicity. *J. Med. Chem.* **2013**, *56*, 8892−8902.
(71) Borenfreund, E.; Puerner, J. A. Toxicity Determined in vitro by Morphological Alterations and Neutral Red Absorption. *Toxicol. Lett.* **1985**, *24*, 119−124.
(72) Singh, N. P.; McCoy, M. T.; Tice, R. R.; Schneider, E. L. A Simple Technique for Quantification of Low Levels of DNA Damage in Individual Cells. *Exp. Cell Res.* **1988**, *175*, 184−191.
(73) Valentin-Severin, I.; Hegarat, L. L.; Lhyguenot, J. C.; Bon, A. M. L.; Chagnon, M. C. Use of HepG2 Cell Line for Direct or Indirect Mutagens Screening: Comparative Investigation Between Comet and Micronucleus Assays. *Mutat. Res., Genet. Toxicol. Environ. Mutagen.* **2003**, *536*, 79−90.
(74) Collins, A. R.; Ai-guo, M.; Duthie, S. J. The Kinetics of Repair of Oxidative DNA Damage (Strand Breaks and Oxidised Pyrimidines) in Human Cells. *Mutat. Res., DNA Repair* **1995**, *336*, 69−77.
(75) Shargel, L.; Wu-Pong, S.; Yu, A. B. C. *Applied Biopharmaceutics & Pharmacokinetics*, 5th ed.; McGran-Hill: New York, 2005; p 811.
(76) DiPiro, J. T.; Spruill, W. J.; Wade, W. E.; Blouin, R. A.; Pruemer, J. M. *Concepts in Clinical Pharmacokinetics*, 5th ed.; American Society of Health-System Pharmacists: Maryland, 2010; p 250.
(77) Zhang, C.; Yuan, X. E.; Li, H. Y.; Zhao, Z. J.; Liao, Y. X.; Wang, X. U.; Su, J.; Sang, S. S.; Liu, Q. Anti-Cancer Effect of Metabotropic Glutamate Receptor 1 Inhibition in Human Glioma U87 Cells: Involvement of PI3K/Akt/mTOR Pathway. *Cell Physiol. Biochem.* **2015**, *35*, 419−432.
(78) Wang, W.; Cho, H.-Y.; Rosenstein-Sisson, R.; Ramos, N. I. M.; Price, R.; Hurth, K.; Schontal, A. H.; Hofman, F. M.; Chen, T. C. Intratumoral Delivery of Bortezomib: Impact on Survival in an Intracranial Glioma Tumor Model. *J. Neurosurg.* **2018**, *128*, 695−700.
(79) Lan, F.; Yang, Y.; Han, J.; Wu, Q.; Yu, H.; Yue, X. Sulforaphane Reverses Chemo-Resistance to Temozolomide in Glioblastoma Cells by NF-κB-dependent Pathway Downregulating MGMT Expression. *Int. J. Oncol.* **2016**, *48*, 559−668.
(80) Zhang, M.; Herion, T. W.; Timke, C.; Han, N.; Hauser, K.; Weber, K. J.; Peschke, P.; Wirkner, U.; Lahn, M.; Huber, P. E. Trimodal Glioblastoma Treatment Consisting of Concurrent Radio-

DOI: 10.1021/acs.jmedchem.8b01305
J. Med. Chem. 2019, 62, 1231−1245

therapy, Temozolomide, and the Novel TGF-β Receptor I kinase inhibitor ly2109761. *Neoplasia* **2011**, *13*, 537−549.
(81) Nukatsuka, M.; Nakawaga, F.; Takechi, T. Efficacy of Combination Chemotherapy Using a Novel Oral Chemotherapeutic Agent, TAS-102, with Oxaliplatin on Human Colorectal and Gastric Cancer Xenografts. *Anticancer Res.* **2015**, *35*, 4605−4616.
(82) Li, M. Y.; Lv, Y. C.; Tong, L. J.; Peng, T.; Qu, R.; Zhang, T.; Sun, Y. M.; Chen, Y.; Wei, L. X.; Geng, M. Y.; Duan, W. H.; Xie, H.; Ding, J. DW10075, a Novel Selective and Small-molecule Inhibitor of VEGFR, Exhibits Antitumor Activities Both in vitro and in vivo. *Acta Pharmacol. Sin.* **2016**, *37*, 398−407.
(83) Kilkenny, C.; Browne, W.; Cuthill, I. C.; Emerson, M.; Altman, D. G. National Centre for the Replacement, Refinement and Reduction of Animals in Research. Animal Research: Reporting in vivo Experiments-the ARRIVE guidelines. *J. Cereb. Blood Flow Metab.* **2011**, *31*, 991−993.
(84) Maciel, I. S.; Azevedo, V. M.; Pereira, T. C.; Bogo, M. R.; Souza, A. H.; Gomez, M. V.; Campos, M. M. The Spinal Inhibition of N-type Voltage-gated Calcium Channels Selectively Prevents Scratching Behavior in Mice. *Neuroscience* **2014**, *277*, 794−805.
(85) Freitas, R. D. S.; Costa, K. M.; Nicoletti, N. F.; Kist, K. W.; Bogo, M. R.; Campos, M. M. Omega-3 Fatty Acids are Able to Modulate the Painful Symptoms Associated to Cyclophosphamide-induced-hemorrhagic Cystitis in Mice. *J. Nutr. Biochem.* **2016**, *27*, 219−232.
(86) West, C. M. L.; Cooper, R. A.; Loncaster, J. A.; Wilks, D. P.; Bromley, M. Tumor Vascularity: A Histological Measure of Angiogenesis and Hypoxia. *Cancer Res.* **2001**, *61*, 2907−2910.

DOI: 10.1021/acs.jmedchem.8b01305
J. Med. Chem. 2019, 62, 1231−1245